PhyMask: Robust Sensing of Brain Activity and Physiological Signals During Sleep with an All-textile Eye Mask

SOHA ROSTAMINIA, SEYEDEH ZOHREH HOMAYOUNFAR, ALI KIAGHADI, TRISHA ANDREW, and DEEPAK GANESAN, University of Massachusetts Amherst

Clinical-grade wearable sleep monitoring is a challenging problem since it requires concurrently monitoring brain activity, eye movement, muscle activity, cardio-respiratory features, and gross body movements. This requires multiple sensors to be worn at different locations as well as uncomfortable adhesives and discrete electronic components to be placed on the head. As a result, existing wearables either compromise comfort or compromise accuracy in tracking sleep variables. We propose PhyMask, an all-textile sleep monitoring solution that is practical and comfortable for continuous use and that acquires all signals of interest to sleep solely using comfortable textile sensors placed on the head. We show that PhyMask can be used to accurately measure all the signals required for precise sleep stage tracking and to extract advanced sleep markers such as spindles and K-complexes robustly in the real-world setting. We validate PhyMask against polysomnography (PSG) and show that it significantly outperforms two commercially-available sleep tracking wearables—Fitbit and Oura Ring.

CCS Concepts: • **Human-centered computing** → **Mobile devices**; **User studies**; • **Computing methodologies** → **Machine learning**; • **Applied computing** → *Consumer health;*

Additional Key Words and Phrases: Sleep monitoring, textile sensors, EEG, EOG, heart rate, respiration, spindle, k-complex

ACM Reference format:
Soha Rostaminia, Seyedeh Zohreh Homayounfar, Ali Kiaghadi, Trisha Andrew, and Deepak Ganesan. 2022. PhyMask: Robust Sensing of Brain Activity and Physiological Signals During Sleep with an All-textile Eye Mask. *ACM Trans. Comput. Healthcare* 3, 3, Article 35 (July 2022), 35 pages.
https://doi.org/10.1145/3513023

1 INTRODUCTION

There has been a significant commercial interest in measuring sleep given the wide-ranging effects of sleep disruptions, which includes diminished cognitive functioning, diabetes, high blood pressure, heart disease, obesity, and depression [46, 57, 62, 66, 103, 109]. There is also growing interest in measuring sleep disorders which affects 50–70 million Americans of all ages and socioeconomic classes [28]. Therefore, it is crucial to scale accurate sleep monitoring such that it can be done less expensively at clinics and more comfortably at home.

This work was funded by the National Science Foundation under agreement CSR Medium 1763524. S.R. and D. G. acknowledge support from the National Science Foundation under agreements 1815347 and 1839999. S.Z.H. and T.L.A. also thank the David and Lucile Packard Foundation for providing partial support.
Authors' address: S. Rostaminia, S. Z. Homayounfar, A. Kiaghadi, T. Andrew, and D. Ganesan, College of Information and Computer Sciences, University of Massachusetts Amherst, Amherst, MA 01003; emails: srostaminia@cs.umass.edu, {shomayounfar, akiaghadi, tandrew}@umass.edu, dganesan@cs.umass.edu.

2637-8051/2022/07-ART35 $15.00
https://doi.org/10.1145/3513023

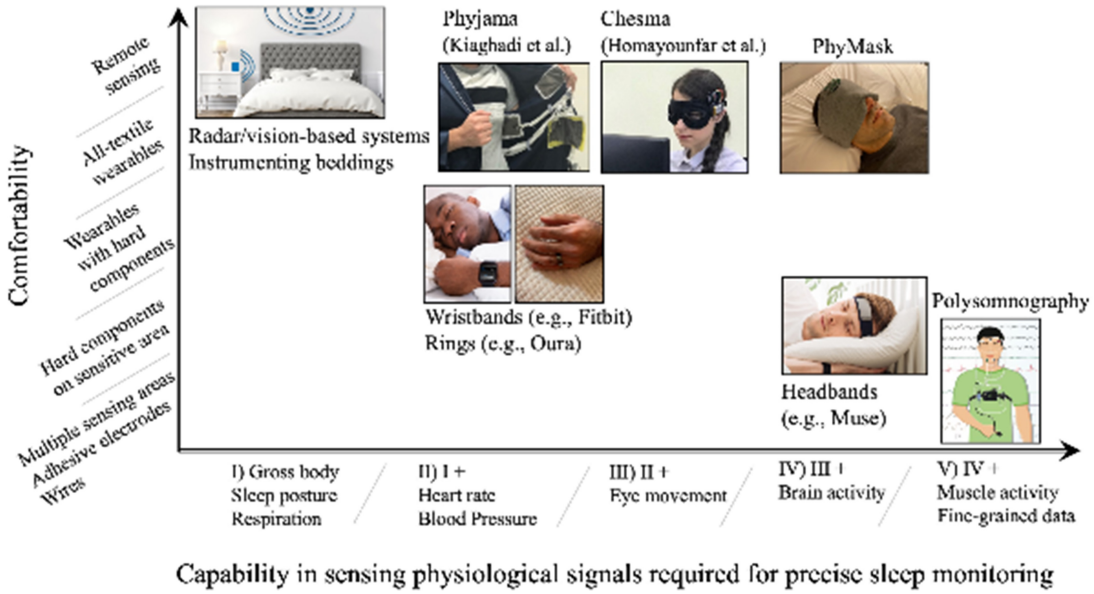

Fig. 1. Comparison of state-of-the-art sleep monitoring solutions in terms of comfort and capability in sensing various signals.

But achieving high-quality clinical-grade sleep monitoring with a comfortable wearable device is complicated by the number of sensor modalities and locations that need to be simultaneously monitored. Sleep is a complex process and monitoring it accurately necessitates many sensors placed at different places on the body. This includes sensors to measure brain activity, eye movement, muscle activity, as well as cardio-respiratory features, and gross body movements. To monitor all of these variables, clinical-grade sleep monitoring systems also referred to as **polysomnography** (**PSG**) place electrodes on the head as well as several other locations on the body. However, this is impractical for daily use.

1.1 Limitations of Sleep Trackers

Sleep sensing devices in the market, therefore, have to tradeoff between comfort and accuracy while monitoring sleep parameters (see Figure 1). A key challenge is that measuring brain electrical activity (**Electroencephalography** (**EEG**), is both the most onerous aspect of sleep sensing (due to the presence of hard sensing components on the head) and the most valuable sensing modality (since sleep is best measured via brain activity).

Measuring surrogate signals: Several efforts on sleep sensing devices favor comfort over accuracy and rely on surrogate measures of sleep such as heart rate, breathing, and body movement signals rather than EEG. Sleep monitors that use surrogate measures of sleep include contactless sleep monitors like instrumented bedding and bedside sleep monitors [59, 68, 74, 94] as well as wearable devices such as the Fitbit and Apple Watch [13, 21].

While these are comfortable, they sacrifice fidelity and precision. Since the surrogate signals only capture a coarse temporal structure of sleep, they provide only coarse-level sleep metrics like sleep quality and, in some cases, macro-structural analysis of sleep such as sleep stages. In addition, metrics provided by these devices are accurate mostly for "normal" healthy individuals and not representative of individuals with sleep disorders [70]. This is because these devices need to compensate for the imprecision of surrogate measures by relying on large population-level data analysis but these measures are erroneous for individuals whose sleep patterns do not follow population averages. For example, **Rapid Eye Movement** (**REM**) sleep stage is known as a state where

the person experiences random/rapid movement of the eyes, accompanied by low muscle tone throughout the body, and the tendency to dream vividly. However, a person who is suffering from the REM sleep disorder usually has violent arm and leg movements during the REM sleep stage. Sleep monitors that use surrogate measures of sleep assume that the body normally freezes and does not move during REM since they solely measure the cardio-respiratory features and gross body movement. As a result, these sleep trackers are inaccurate for individuals with substantial clinical needs such as older adults with sleep disorders and medication-induced sleep disruptions [61]. They also fail to capture day/night (circadian) rhythm sleep patterns of individuals with sleep abnormalities (such as older adults with dementia) [116].

Measuring EEG signal: Other sleep trackers focus on accuracy and measure EEG but sacrifice comfort in the process. Such head-worn devices with electrodes include headbands and masks that have become available for sleep tracking [11, 15, 22]. However, the challenge in these devices is comfort—head-worn sleep trackers require rigid sensing elements that are directly pressed against the skin. For example, the Phillips Smart Sleep headband [18] uses behind-the-ear sticker electrodes and the Muse [15] has an optical sensor on the forehead and EEG electrodes on a rigid frame. These rigid structures and the embedded hard components on the head make such a device unnatural and uncomfortable.

Another important limitation of these devices is that despite measuring EEG, these devices do not currently expose micro-structures of sleep such as spindles and K-complexes. This is a missed opportunity since micro-structures play an essential role in information processing and long-term memory consolidation [58] and potentially as biomarkers of Alzheimer's disease [60] and seizures [45].

1.2 Our Contribution

In this work, we present a complete textile-based head-worn sleep sensing system that bridges the gap in existing sleep measurement devices in two ways. First, we show that a single head-worn device that leverages solely textile-based sensors can provide nearly all the parameters that are used in clinical-grade sleep monitoring without requiring rigid sensing elements and thereby without sacrificing comfort. Second, we show that such a device can provide accurate estimates of both macro and micro-structures of sleep including sleep stages, spindles, and K-complexes.

Our work builds on our previous efforts on developing individual sensors that provide part of the solution. In the previous work [53], we have introduced two sensors that we leverage in this work: (a) a new thread-based, reusable wet electrode that achieves the high signal quality of commercial wet electrodes as well as the comfort and unobtrusiveness of dry electrodes (our preliminary results showed that these electrodes were viable for measuring eye movement patterns), and (b) a fabric-based piezoionic pressure sensor [52] that is sensitive to ballistic signals from heartbeats.

In this work, we build on the above to provide a holistic multi-modal solution that can provide reliable and robust measures of sleep in a natural setting. Our work makes notable contributions towards a practical daily-use system that is comfortable yet accurate. From a device perspective, we show for the first time that (a) a fabric-based electrode can be used to accurately measure EEG signals with high signal-to-noise, and that (b) textile-based pressure sensors on the sleep mask can allow us to sense tiny head movements induced by heartbeats and respiration in various sleep postures. From an analytic perspective, we describe a signal processing and machine learning pipeline that allows us to extract both high-level physiological features such as heart rate and breathing rate, as well as micro-events of brain activity during sleep such as spindles and k-complexes. Put together, PhyMask is a comfortable textile-based sensing platform that can simultaneously sense brain activity EEG, eye movement **electrooculography** (**EOG**), physiological parameters (respiratory and cardiac rhythm), gross body movement, and sleep posture from the head and infer both macro- and micro-structural parameters of sleep.

We design and fabricate a fully functioning prototype of a comfortable all-textile sleep tracking device (shown in Figure 2) that includes the fabric-based sensing elements, fabric-based wires, low-power circuit for signal

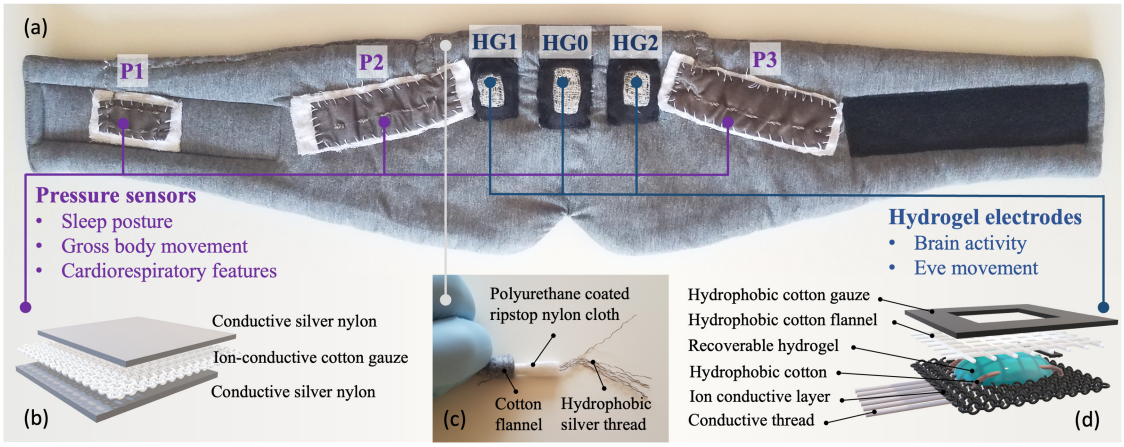

Fig. 2. PhyMask platform. (a) inside view of PhyMask, illustrating pressure sensors and hydrogel electrodes placement, (b) schematic of the layered structure of pressure sensor, (c) wiring constructed with isolated hydrophobic conductive threads, and (d) the schematic of the layered structure of hydrogel electrode.

amplification and data acquisition, a wireless radio for data transfer, and tailored algorithms for physiological signals and sleep micro-events tracking.

We perform exhaustive data collection studies to validate our device and compare it against polysomnography ground truth and two popular sleep trackers, Fitbit wristband and Oura Ring, for continuous long-term sleep tracking.

Our results show that:

— We have high accuracy for measuring heart rate (median error of 1.7 beats/minute) and respiration (median error of 1 resp/minute), and can easily capture gross motor activity including posture changes.
— The PhyMask can measure sleep stages almost as well as polysomnography ground truth with an F1 score of 0.91, and greatly outperforms Fitbit (F1 score of 0.64) and Oura Ring (F1 score of 0.7).
— The PhyMask can be used to detect advanced sleep markers such as spindles and K-complexes that are typically not provided by commercial wearable devices. We show that PhyMask detects spindles and K-complexes with the accuracy of 85% and 86%, respectively.

2 BACKGROUND AND RELATED WORK

In this section, we first look at the key sleep markers that we need to measure to provide a reliable sleep tracking solution. We then look at the existing sleep tracking solutions. We explain the PhyMask solution and how it overcomes the accuracy and aesthetic shortcomings of current state-of-the-art sleep tracking devices.

2.1 Background: Sleep Structure and Biosignal Characteristics

Sleep Macro- and Micro-structure: Traditional sleep measures tend to focus on sleep macrostructure i.e., the longer-term measurements of sleep. A number of parameters are commonly used as outcome measures of sleep macrostructure including **total sleep time** (**TST**), sleep latency, sleep efficiency, wake time, and percentage of Stage 1 (N1), Stage 2 (N2), Stage 3 (N3) and REM sleep.

However, sleep is also rich in shorter timescale phasic EEG events such as K-complexes, spindles, delta wave bursts, and others [78, 110]. While macrostructural variables have received more attention in past research, recent work has paid more attention to microstructural variables due to important clinical correlations to

Table 1. The Characteristics of Important Biosignals used in Sleep Analysis During Each Sleep Stage [97]

Sleep stage	Brain activity (EEG)	Eye movement (EOG)	Heart rate	Respiration	Gross motor activity
N1	Theta (4–8 Hz)	Slow cyclic eye rolling	↓	↓	Occasional muscle twitches
N2	Theta (4–8 Hz) spindles & K-complexes	↓	↓	↓	↓
N3	Delta (0.5–4 Hz)	Lowest	Lowest	Lowest	Relaxed
REM	Beta (13–32 Hz)	fast rapid eye movement	↑	Fast & irregular	Paralysis

age-related sleep changes and other age-related disorders like Parkinson's and Alzheimer's [108]. Many age-related sleep changes are not captured by traditional sleep stage scoring—for example, research has shown that ageing-related changes were reflected particularly in fast spindle density, K-complex density, and delta power during N3 sleep—than on conventional sleep staging variables [104].

Biosignal characteristics during sleep: A number of biosignals need to be measured to fully characterize micro and macro-structural parameters of sleep. Table 1 summarizes the biosignals characteristics during each sleep stage i.e., REM, non-REM N1, non-REM N2, and non-REM N3. Each sleep stage is characterized by brain waves of specific frequencies and/or amplitudes and is also associated with certain types of eye movements and muscle activities. Therefore, brain activity EEG, eye movement EOG, and muscle activity **electromyographic (EMG)** measurements are required for accurate sleep staging. Brain activity, in particular, is considered the most important signal for high-quality sleep stage monitoring [97].

Laboratory-based PSG, which is considered the most clinically accurate method of monitoring sleep also includes monitoring of several other parameters which are relevant to the holistic understanding of sleep. Cardio-respiratory parameters are particularly useful for studying and analysis of sleep disorders such as apnea. Thus, measurements of respiration and heart features are also included in laboratory-based PSG. In addition, gross body movements during sleep are also important when studying sleep disorders such as periodic leg movements.

2.2 State-of-the-art in Sleep Tracking

There is a vast body of literature on sleep tracking solutions (surveyed in [41, 56, 63, 67, 82]). Our core contribution is the development and evaluation of an unobtrusive all-textile sleep monitoring solution that can capture all signals of interest to sleep. Hence, we focus our literature survey on other relevant efforts with respect to two questions: (a) which of these sleep markers can these solutions provide? and (b) how comfortable and unobtrusive are these techniques?

Due to the size and complexity of the literature on this topic, it is difficult to find simple categories within which all of the related studies fit comfortably. For the purposes of comparison with our work, we classify the related studies into three categories based on the form factor: (1) non-wearable sleep trackers, (2) wrist-worn wearable sleep trackers, and (3) head-worn wearable sleep trackers. The comparison between PhyMask and existing state-of-the-art systems is summarized in Table 2.

Non-wearable sleep trackers. There has been a number of non-wearable sleep tracking approaches that attempt to monitor sleep indirectly by instrumenting the environment around the user. For example, Jia et al. leverage highly sensitive geophones and embed them into bedding to measure the seismic motions induced by individual heartbeats and slow-moving signals from respiration [59]. Commercial MEMS accelerometer-based and piezoelectric-based units are also available, that can measure body movement and heart rate based on ballistocardiography signals measured via the bed during sleep [6, 10]. Several approaches also use vision-based and

Table 2. Comparison of the State-of-the-art Physiological Signals Monitoring Solutions in the Context of Sleep

Work	EEG EOG	Heart rate Respiration	Other biosignals	Sleep stages	Comfort	Form factor
Jia et al. [59]	×	✓	×	None	✓Non-wearable	Bedding
Beddit* [10]	×	✓	Snoring	Sleep/Wake	✓Non-wearable	Bedding
Li et al. [68]	×	✓	×	None	✓Non-wearable	Camera
Vogels et al. [113]	×	✓Heart rate × Respiration	SpO_2	None	✓Non-wearable	Camera
Deng et al. [44] Yu et al. [118]	×	× Heart rate ✓Respiration	Head posture Body Movement	None	✓Non-wearable	Camera
Nochino et al. [89]	×	×	Body Movement	Light, Deep, REM, Wake	✓Non-wearable	Camera
Rahman et al. [94]	×	✓	Body movement	Non-REM, REM, Wake	✓Non-wearable	Radar stand
SleepScore Max* [20] Zhao et al. [120]	×	× Heart rate ✓Respiration	Body movement	Light, Deep, REM, Wake	✓Non-wearable	Radar stand
Liu et al. [74]	×	✓	×	None	✓Non-wearable	WiFi stand
Liu et al. [75]	×	× Heart rate ✓Respiration	Body movement Sleep posture	None	✓Non-wearable	WiFi stand
Oura* [17]	×	✓	Temperature Body movement	Light, Deep, REM, Wake	× Wearable rigid structure	Ring
Fitbit*, Garmin*, Whoop* [13, 14, 23]	×	✓	Temperature, SpO_2, Body movement	Light, Deep, REM, Wake	× Wearable rigid structure	Wristband
Apple watch* [21]	×	✓	Body movement SpO_2	Sleep/Wake	× Wearable rigid structure	Wristband
Actiwatch*, Polar* [9, 19]	×	✓	Body movement	Sleep/Wake	× Wearable rigid structure	Wristband
Ye et al. [117]	×	✓Heart rate × Respiration	Body movement	N1, N2, N3, REM, Wake	× Multi-systems rigid structure	Wristband Pillow
Kim et al. [65]	✓	×	×	Light, Deep, REM, Wake	× Wearable rigid structure	Headband
Lin et al. [72]	✓	×	×	N1, N2, N3, REM, Wake	× Wearable rigid structure	Headband
Phillips Smartsleep* [18]	✓	✓	×	N1, N2, N3, REM, Wake	× Wearable rigid structure	Headband
Muse* [15]	✓	✓	Head posture	Light, Deep, REM, Wake	× Wearable rigid structure	Headband
dreem* [11]	✓	× Heart rate ✓Respiration	Head posture Body movement	N1, N2, N3, REM, Wake	× Wearable rigid structure	Headband
Brainbit* [22]	✓	×	×	Sleep/Wake	× Wearable rigid structure	Headband
Nakamura et al. [86]	✓	×	×	N1, N2, N3, REM, Wake	✓ Wearable **All-fabric**	In-ear
Nguyen et al. [87]	✓	×	Facial EMG	N1, N2, N3, REM, Wake	✓ Wearable **All-fabric**	In-ear
Kiaghadi et al. [64]	×	✓	Sleep posture Body movement	None	✓ Wearable **All-fabric**	Pajamas
Liang et al. [69]	× EEG ✓EOG	×	×	Light, Deep, REM, Wake	✓ Wearable **All-fabric**	Eye mask
PhyMask	✓ + Spindle/ K-complex	✓	Head posture Body movement	N1, N2, N3, REM, Wake	✓ Wearable **All-fabric**	Eye mask

The commercialized systems are marked with *.

depth camera-based methods to find physiological variables such as respiration [31, 81], heart rate [68], pulse oximetry [113], head posture [44], and body movement [89, 118] during sleep. Another body of work is on radar-based sensing of respiration and heart rhythm [25, 54, 88, 94]. These methods use FMCW or UWB radars and measure changes in the displacement and the Doppler shifts due to respiration and ballistics of the heart.

While non-contact sleep tracking solutions have the advantage of being unobtrusive and comfortable, they tend to be imprecise and noisy. The imprecision stems from the inability to observe the most valuable signal for sleep monitoring i.e., EEG, and relying on other parameters such as body movements (chest movement during respiration and gross body movements) to infer sleep markers [101]. Noisy measurements result from the fact that the signal is confounded by proximate activity such as multiple individuals on the bed [59, 74] or other moving objects in the vicinity like a fan.

Wrist-worn wearable sleep trackers. There are many wearable devices in the market for sleep sensing, most of which use hard electronic components such as **photoplethysmography (PPG)** and IMU to measure the pulse wave and body movement on the wrist or fingers (e.g., Fitbit [13], Garmin [14], Actiwatch [9], Whoop [23], and Oura Ring [17]).

The main disadvantage of these solutions is the inability to monitor the EEG and EOG signals, which is considered critical for high-quality sleep analysis. Hence, they solely rely on cardiac, respiratory, and gross body movement information for sleep stage tracking which results in poor performance. This can also affect their ability in detecting shorter-time sleep, i.e., nap [41]. Several studies in research settings have reported on the validity of the wearable sleep trackers compared to PSG [37, 80, 93, 112]. For example, Moreno-Pino et al. validate two models of Fitbit sleep trackers (Charge 2 and Alta HR) against PSG and find statistically significant differences between PSG and Fitbit measures for all sleep stages except for REM sleep [84]. Also, Miller et al. examine Whoop against PSG and report the sensitivity to light sleep, deep sleep, REM, and wake, 62%, 68%, 70%, and 51% respectively [83].

Head-worn wearable sleep trackers. Another category of sleep tracking devices is head-worn wearables. Head-worn solutions are more promising as they allow us to obtain biopotential signals (EEG and EOG) from the head. Kim et al. leverage gel-based standard adhesive electrodes on a headband device and collect EEG, EOG, and EMG signals for sleep tracking purposes [65]. Phillips Smartsleep [18] also use sticky disposable electrodes placed behind the ear and obtain EEG signal during sleep. Despite the high signal quality of these electrodes, they are uncomfortable due to the adhesive and are not practical for long-term wear, since once the gel dehydrates, the electrode loses its functionality and should be replaced. Therefore, dry electrodes are often preferred in wearable devices. Kuo et al. use graphene-based electrodes in a sleep mask, for tracking eye movement signals during sleep [69]. Lin et al, developed a headband encapsulating dry electrodes to study EEG for monitoring sleep, predicting headaches, and treating depression [72]. Furthermore, the commercially available computational headbands such as Muse [15], dreem [11], and Brainbit [22], use dry electrodes for obtaining EEG on the forehead. They also have a PPG sensor for cardiac and respiration rate tracking and other sensors. Among the head-worn wearables, in-ear sensors have also gained much interest lately [27, 79, 87]. For example, Nakamura et al. [86] leverage in-ear EEG flexible sensor for overnight sleep stage monitoring. In a recent study [107], Shustak et al. developed a temporary-tattoo dry electrode system for capturing EEG, EOG, and EMG during sleep.

The main drawback of these systems is the rigid structure of the device and the use of hard sensing components that touch the skin on the sensitive head areas. These can make the system highly uncomfortable in different sleep postures and not ideal for continuous long-term sleep tracking. Another debatable aspect of the current head-worn solutions is the quality of the acquired biopotential signals. The majority of these technologies use dry electrodes to avoid adhesives and increase the comfort factor, however, this results in a considerable increase in motion artifact [71, 98].

PhyMask. While most of the current solutions focus on collecting a few of the essential signals needed for precise sleep monitoring, PhyMask captures all these signals i.e., EEG, EOG, and heart and respiratory rate, while providing information on head posture and body movements.

This allows our device to extract information about sleep macrostructure as well as microstructure in contrast to existing devices which only provide macrostructural parameters. To the best of our knowledge, PhyMask is the first sleep tracking system that can also accurately detect sleep micro-events, i.e., Spindle and K-complex in addition to macrostructural parameters.

2.3 State-of-the-art Textile-based Wearables

Since PhyMask relies on textile-based sensing elements, we look at state-of-the-art textile-based sensing solutions for monitoring these parameters.

Physiological and physical signals sensing. Physiological and physical sensing through fabric-based elements has gained a lot of interest during the past decades. Some of the existing methods and requirements of smart textiles are surveyed in [29]. Many of these devices are based on conductive fabric electrodes embedded into tight-fitting clothing. There has been some work on measuring impedance changes for physiological measurements—for example, [91] integrates piezoelectric elements in a garment and acquires electrocardiogram, respiration, and activity information. In our previous work, Phyjama [64], we also showed that we can measure heart rate and respiration as well as sleep posture through resistive pressure and triboelectric patches are sewn into loosely worn sleepwear. To the best of our knowledge, PhyMask is the first system that captures the physiological and physical signals (cardiac, respiration, general body movement, and head posture) through fabric-based elements robustly from the *head*.

Biopotential signals sensing. There have been some studies on the design of textile-based dry electrodes. For example, silver-coated [69] or graphene-coated [48, 99] fabrics, or polymeric foams [73] have been embedded as a dry electrode into a head-worn to obtain EOG and EEG signals. Pani et al. [90] use PEDOT: PSS-based electrodes to measure ECG signals. While dry electrodes are unobtrusive and comfortable to use, they are highly susceptible to noise. The fundamental challenge in reliably extracting biopotential signals through wearable electrodes is to design an electrode enjoying both the signal quality of traditional wet electrodes and the comfort of the dry ones. Shu et al. [106] and Alba et al. [26] a propose semi-wet textile electrodes for EEG measurement. However, to the best of our knowledge, the existing solutions do not have the longevity, wash-stability, and recoverability that are required for long-term use of the electrodes.

PhyMask. PhyMask presents a complete system that incorporates several of these textile-based sensor innovations in a single platform to monitor sleep. PhyMask uses the thread-based, reusable wet electrode to measure biopotential signals that have the signal quality of commercial wet electrodes and the comfort and unobtrusiveness of dry electrodes. We also use a pressure-sensitive, ionic fabric electrode to capture pulse wave-forms from the head. In order to further minimize using discrete electronic hard components at sensitive pressured locations, we inter-connect the all-textile patches by using silver-plated nylon threads as wires that are shielded in cotton.

3 PhyMask OVERVIEW

A key design objective of PhyMask is to sense the biosignals relevant to sleep while eliminating all hard sensing components and relying solely on textile-based and soft sensing elements that can be embedded in a sleep mask. While it is possible to obtain sleep markers using a combination of devices, say one on the head for EEG and EOG [15, 18], and another on the body for cardio-respiratory rhythm and movement [17, 64], it is more ideal to obtain all metrics from a single device on the head. Since the head area is sensitive, we remove all hard sensing components from the head-worn device and rely solely on textile-based and soft sensing elements that can be embedded in a sleep mask. Such a design can eliminate rigid sensing elements from being in direct contact with the skin on the head area. We note that, unlike sensing elements that need to be in contact with the skin, other rigid components like the microcontroller, radio, and battery are easier to place in a more conducive location. We now describe the design of such a device and how we optimized it to extract the markers of interest.

3.1 Robust Sensing of Biopotential Signals with Textile Electrodes

In order to extract biopotential signals such as EEG and EOG in a comfortable manner, we need a fabric-based electrode that is comfortable, robust, and provide reliable high **signal-to-noise ratio** (**SNR**). PhyMask leverages a recent innovation; a fabric-based, reusable wet electrode that has a layer of composite hydrogel, which when hydrated, mechanically behaves like the foams used in the standard electrodes [53]. This is sufficiently

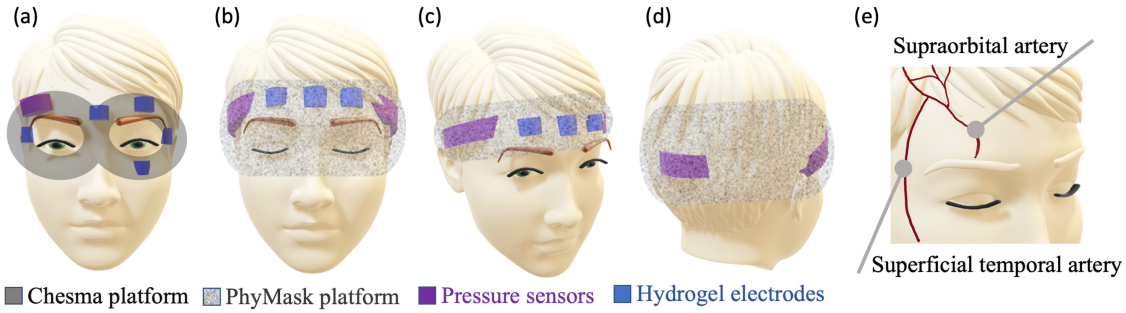

Fig. 3. Schematic drawings. (a) illustrates the sensors placements on our previous work, Chesma platform [53]. (b) Front, (c) side, and (d) rear views of PhyMask's sensors placements are depicted. As it is shown in (c), PhyMask can be built in the form factor of both headband and eye mask. (e) illustrates schematic drawings of supraorbital and superficial temporal arteries.

cushion-like to minimize motion artifacts in the absence of any harsh skin adhesives. The advantage of these electrodes is that they overcome the aesthetic drawback of requiring adhesives to have contact with the skin while simultaneously providing strong signal integrity. In addition, they address the lack of reusability of the commercial wet electrodes.

In order to reduce the computational cost of the system, we need to choose the minimum number of electrodes that can be embedded into a sleep mask and provide reliable EEG and EOG signals concurrently. The typical electrode placement for EOG and EEG can be too complex. For example, EOG alone requires five electrodes placed as illustrated in Figure 3(a).

To reduce the number of electrodes, we look at a more restricted placement. In order to be able to capture strong EEG signals, the electrodes should be placed closer to the brain area. Thus, we place one electrode on top of each left and right eyes (HG1 and HG2, respectively) and one in the middle (HG0), serving as both reference and common ground (shown in Figure 3(b)). HG1 and HG2 electrodes are respectively closest to the Fp1 and Fp2 sites (illustrated in Figure 13) according to the standard 10–20 EEG recording guideline [24] and can conveniently capture horizontal EOG signal which is sufficient for the purpose of sleep stage tracking.

3.2 Robust Fabric-based Physiological Signals Sensing on the Head

The next question is how to obtain robust physiological signals such as pulse and breathing, as well as gross motor activity on the head using comfortable textile-based sensing elements.

Traditional methods for capturing cardiac signals on the head focus on placing sensors at the supraorbital artery position (shown in Figure 3(e)). The cardiac signal at this location can be measured with rigid optical sensors to obtain PPG (e.g., the MUSE headband). Furthermore, in the prior work on textile-based sensors, we have looked at using this artery to obtain pulse due to pressure changes (Chesma [53]). However, the issue is that textile pressure sensors do not work well when the signal is present in a small surface area like a single artery. This leads to a weak and noisy signal that is highly sensitive to small changes in sleep position.

We address this limitation using a new method for measuring cardiac signals in the head area while using textile-based sensors. A key observation that we make is that the cyclical movement of blood from the heart to the head via the abdominal aorta and the carotid arteries causes the head to move imperceptibly in a periodic manner. Similar oscillations can also be observed during respiration since each inhale and exhale action results in body movements [30]. Therefore, unlike the previous work which attempts to sense the artery pulse in a very localized region, we leverage fabric-based pressure sensors across a larger surface area to measure both the pressure exerted by blood pulsing through the facial artery as well as the small subtle head vibrations caused by blood pumping and respiration.

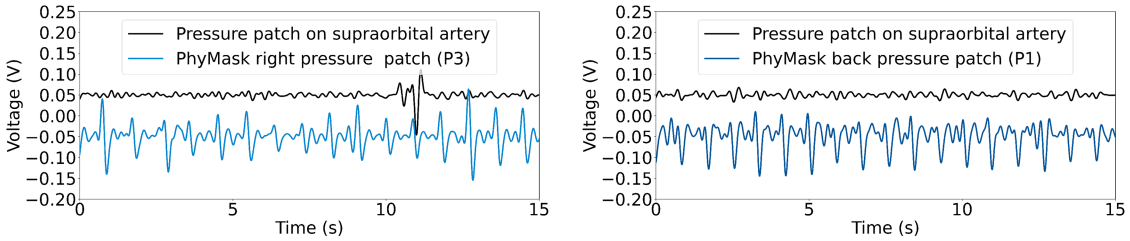

(a) lying on right. (b) lying on back.

Fig. 4. Comparing the measured pulse signal at a single location versus over a broader surface area in PhyMask platform, when the user is lying on their right and back, respectively. While the pressed pressure patch of the PhyMask platform provides a reliable pulse signal, the pressure patch placed on the supraorbital position fails in providing robust signal.

In order to detect these vibrations under various sleep postures, we place the pressure patches on the back (P1), left (P2), and right (P3) of the sleep mask, where at least one of the patches is pressed on the pillow under the user's head weight in different sleep postures (shown in Figure 3b–d). For precise placement of the pressure sensors and in order to achieve the maximum heart rate sensing ability, we look more closely at the physiology of the head. Figure 3e illustrates the anatomy of the arteries passing through the head. The superficial temporal artery is a major artery of the head. It arises from the external carotid artery when it splits into the superficial temporal artery and maxillary artery. Its pulse can be felt above the zygomatic arch, above and in front of the tragus of the ear. Therefore, P2 and P3 sensors are made bigger and placed slightly tilted (~15°) on the temple area, allowing for the pulse waveform from the frontal branch of the superficial temporal artery to be measured. This layout of the sensors also enables detecting the head posture on the pillow and can capture the pressure changes caused by gross body movement.

The difference between measuring pulse at a single location versus measuring head oscillations over a broader surface area is illustrated in Figure 4(a) and (b), where the participant is lying on their right and back, respectively. We see that the pulse signal acquired with the sensors placed on the supraorbital artery is weak and imprecise, while PhyMask's sensors that are optimized to extract head oscillations can pick up a clear pulse signal.

3.3 Fabrication of PhyMask

Figure 2(a) shows the integrated PhyMask platform, which incorporates three biopotential electrodes and three pressure sensors. We made two biopotential electrodes with a functional area of 1 cm × 1 cm and one electrode with a functional area of 1 cm × 2 cm, serving as a reference. We made the reference electrode slightly bigger to ensure better skin-electrode contact and hence a more stable signal during long wear. The layered structure of the electrode (shown in Figure 2(d)) is comprised of an array of conductive silver-plated nylon threads, serving as the charge collector, on top of hydrophobic backing fabric. This conductive array is then coated with silver chloride that provides the ion conductivity required for transducing signals from the ionic form in the body to the electrons in the wires. By taking advantage of the **initiative chemical vapor deposition** (**iCVD**) of **poly(hydroxyethyl acrylate)** (**pHEA**) on a pharmaceutical-grade silver gel, we developed a reusable composite hydrogel on top of the electrode. Finally, open-weave cotton gauze is placed on top and a cotton flannel framed the hydrogel to protect it from mechanical abrasions. The wide pores of the gauze fabric enable rehydration of the hydrogel and its direct contact with the skin while protecting it from being rubbed away. All the fabrics used in this electrode are coated with poly(perflurodecyl acrylate) using iCVD. The hydrophobic nature of this polymer prevents the fabrics from absorbing water/perspiration rather than the hydrogel. The wash stability of the biopotential electrodes is validated in our previous study [53], showing their durability and high signal quality even after 15 home-laundering operations.

As it can be seen in Figure 2(b), the pressure sensor is comprised of an ion conductive active layer sandwiched between two silver-coated conductive fabrics as electrodes. The active layer is made of a cotton gauze fabric coated with a poly(siloxane) polymer, poly(N-propylsilyl-N,N,N,-trimethylammonium chloride) through a solution-phase functionalization process. Through the application of compression stress on the sensor, the mobile chloride counterions relocate on the surface of the fabric and the ions movement in addition to the reduction of the air gap between the layers lead to a decrease in the impedance of the pressure sensor. The functionalized ion-conductive layer was further encapsulated with a poly(perfluoroalkylsiloxane) coating through iCVD. The hydrophobic nature of this coating protects the ion-conducting fabric against common aging processes, such as erosion during laundering or air oxidation, ensuring that the ionic conductivity of the sensor will not be washed away or diluted if the pressure patch comes into contact with sweat [53]. We made a large patch of functionalized ion-conductive layer, and then cut it into four 12 cm × 4 cm and two 6 cm × 4 cm sheets, each of which was sewn around the perimeter onto a sheet of silver fabric. Sewing together each pair of these joined gauze-silver sheets yielded three resistive sensors with a four-layer structure. In terms of washability of the pressure sensors, our experiments results in [53, 115] bear testimony to the fact that the resistive patch can withstand up to 20 home-laundering operations.

All of these fabric electrodes and sensors are tightly sewn onto a commercially-available sleep mask—purchased from Amazon 4.5/5 with more than 4,000 reviews, it was chosen because of its lightweight and adaptability to a wide variety of head shapes and sizes. For maximum comfort and to minimize the number of hard electronic components, we avoided using wires in our design. Instead, we used silver-plated nylon threads. In order to shield our wiring system from electromagnetic noises and make it laundering-stable, we cladded the silver threads with a three-layer fabric-based shield, comprising of polyurethane-coated ripstop nylon cloth as the first layer, followed by a nanoscale (40–50 nm) coating of a hydrophobic polymer, PFDA as second, and encased within cotton piping as the last layer (shown in Figure 2(c)). Our wiring system serves as lightweight and flexible interconnects between the six sewn-on electrodes and the circuit board (PCB) microcontroller (MCU).

4 PhyMask SYSTEM DESIGN

The PhyMask system pipeline have two main components: (1) the software running on a host device to process the raw data and extract the sleep and physiological features of interest, and (2) the hardware for acquiring sensors signals and real-time Bluetooth communication. In this section, we explain these components in detail.

4.1 PhyMask Processing

We start by describing our methodology for sleep micro-events (i.e., spindle and K-complex) detection from biopotential signals, as well as sleep posture, respiratory, and cardiac rhythm extraction from the pressure signals.

4.1.1 Sleep Spindle and K-complex Detection. As discussed earlier, one of the main advantages of acquiring the EEG signal during sleep is that we can detect and analyze the sleep micro-events such as spindle and K-complex. This is important since their characteristics, e.g., frequency of their occurrence, can unveil a great amount of information regarding the cognitive state of the mind [51]. In this section, we describe the PhyMask approach for detecting spindles and K-complexes in detail.

Sleep spindles are brief bursts of neural oscillations (9–16 Hz, (0.5–3 seconds) generated by the interplay of the thalamic reticular nucleus and other thalamic nuclei during NREM sleep (N2 and N3 stages) [40] (an example is shown in Figure 5(c)). Like spindle, K-complex is a great hallmark of NREM sleep stage 2 and is often followed by a sleep spindle. K-complexes are generated in widespread cortical locations though they tend to predominate over the frontal parts of the brain. K-complex characteristics are very different from spindles. They consist of a brief negative sharp wave immediately followed by a positive component, creating slow-wave (0.8 Hz) and delta (1.6–4.0 Hz) oscillations of 0.5–3 seconds in duration [34] (an example is shown in Figure 5(c)). We train two different models of the same architecture for the detection of spindles and K-complexes. Several classification algorithms

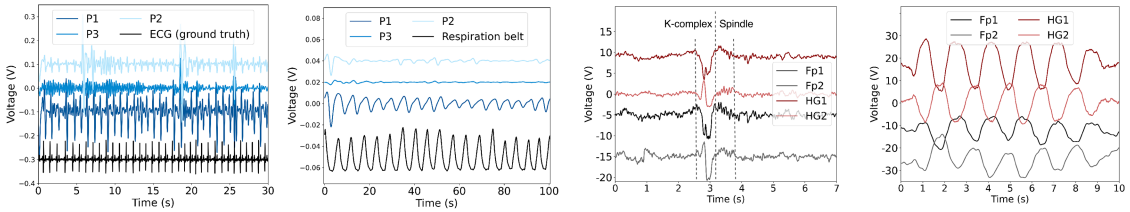

(a) BCG (b) Respiration (c) EEG (d) EOG

Fig. 5. PhyMask signals. (a) The BCG signal is captured by the pressure patches along with the ECG ground truth. (b) The breathing signal along with the ground truth collected with respiration belt. In both (a) and (b) scenarios the user is lying on their back, hence the back patch captures stronger cardiac and respiratory signals. (c) EEG signals captured from the right and left hydrogel electrodes along with the ground truth signals captured from standard wet electrodes. A K-complex followed by a spindle is presented at time 3 seconds. (d) The EOG signal along with the ground truth signals. In this example, the user is looking at right and left repeatedly with eyes closed.

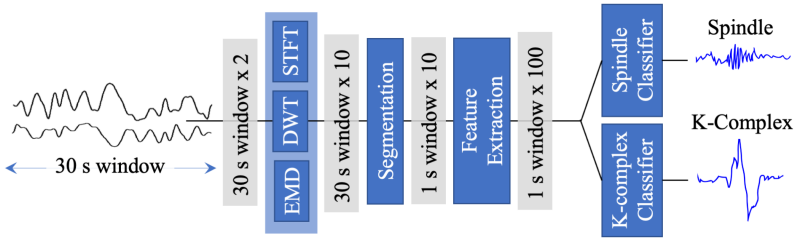

Fig. 6. PhyMask spindle and K-complex detection algorithm pipeline.

were tested during this study, including random forests, neural networks, and support vector machines. We found the random forest classifier to provide the best performance considering our limited dataset size.

We designed two random forest classifiers each for binary spindle/non-spindle and K-complex/non-Kcomplex detection tasks. In order to prepare the data for our binary random forest classifiers, we first apply a 5th order Butterworth filter with a passband of 0.5–35 Hz to filter out noises from the EEG streams. Then, we extract features in both time and frequency domains. Our feature extraction pipeline has two steps (summarized in Figure 6). First, we derive **Short-time Fourier Transform** (**STFT**), **Discrete Wavelet Transform** (**DWT**), and **Empirical Mode Decomposition** (**EMD**) features from 30-second epochs of the EEG stream and append them as additional channels to the original raw signal. In the second step, we extract statistical features from overlapping windows of the output signal of step 1. We empirically choose an input window size of 1 second (125 samples) and the step size of ~0.1 ms (12 samples) for both spindle and K-complex detection. In the following, we describe the details of our feature extraction pipeline.

Short-time Fourier transform (STFT). In the literature, STFT is widely used as one of the main features for automatic spindle and K-complex detection [39, 92, 119]. STFT computation algorithm divides the input vector into overlapping shorter segments of equal length and then the Fourier transform is computed separately on each segment. The output is a 3-dimensional time series containing information regarding the frequency content of each time segment. Given the different frequency characteristics of spindle and K-complex, we extract two separate features from STFT for each event. For our binary spindle detection classifier, since the spindle has a frequency content of 9–16 Hz, we extract (1) the sum of the powers of frequency components of the signal in 10–12 Hz, and (2) the sum of the powers of frequency components of the signal within 9–16 Hz of the signal. For K-complex, which has most of its frequency content around 0.8 Hz and within 1.6–4.0 Hz, we extract (1) the

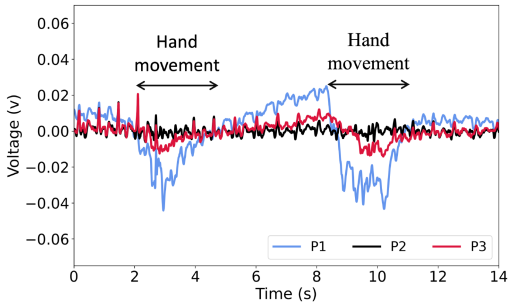

Fig. 7. DC-removed pressure patches signals are illustrated when the user is lying on their back and swinging their hand in time 2–4 seconds and 9–11 seconds. The periodic small spikes on the signals correspond to the heartbeats.

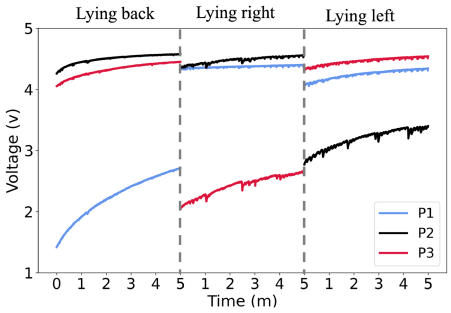

Fig. 8. Pressure patches baseline across postures. The slow oscillations on the signal correspond to respiration while the more choppy ones represent gross body movement.

sum of the powers of frequency components of the signal within 0.5–1 Hz, and (2) the sum of the powers of frequency components of the signal within 1.5–4.5 Hz, from the input windows. We then up-sample the outputs to generate a time series of the same length as the original EEG signal and augment them with the raw EEG stream as additional channels.

Discrete Wavelet transform (DWT). To further investigate the frequency content of the EEG time-series data, we use DWT [105]. DWT obtains low-frequency resolution and high-frequency information using long- and short-time windows, respectively. Because of this, DWT is appropriate for the analysis of the non-stationary signals such as EEG [119]. 2-level DWT and **Daubechies-2** (**db2**) mother wavelet is used in our computation, and the second-level coefficients are taken as the output. The output is up-sampled and appended to the raw EEG and extracted STFT features.

Empirical Mode Decomposition (EMD). EMD can be used for nonlinear and non-stationary signals such as EEG [55]. In this method, a signal is divided into substatements referred to as **intrinsic mode functions** (**IMF**) and sub piece (residue). The main idea behind EMD is to locally reconstruct a signal. The reconstruction is a sum of a local trend and detail. The local trend implies the low-frequency components of the signal (residual), while the local detail IMF is the high-frequency parts. According to this method, a signal is recursively separated step by step. Then a certain number of IMFs and residuals are obtained depending on the content of the signal. We choose the first IMF component as the output and then append it to the output of the previous step. Yücelbaç et al. [119] has also utilized EMD for automatic spindle detection. In their solution, they apply binary thresholding on the first IMF component derived from the EMD of a single EEG stream to detect spindle events.

Statistical feature extraction. In this step, we chunk the output of the previous step, i.e., a multi-channel signal consisting of the raw EEG, extracted STFT features, DWT features, and the EMD components, into overlapping 1-second windows and then extract statistical features including maximum, mean, median, standard deviation, sum, energy, mean-crossing, interquartile range, 10th percentile, and 90th percentile. Finally, in order to train our random forest classifier, we use SMOTE [35] to balance the training dataset.

4.1.2 Gross Motor Movement and Posture Estimation. PhyMask can easily measure pressure changes that reflect the gross motor movement of the limbs. We illustrate by looking at voltage changes of the PhyMask pressure patches when a user moves their hand. Figure 7 shows the DC-removed pressure signal for the three patches when the user is lying on their back. As the user moves their hand during time 2–4 seconds and 9–11 seconds, the pressure signals voltage, especially for the pressed patch, changes dramatically. Please note that the small periodic spikes on the signals correspond to the heartbeats.

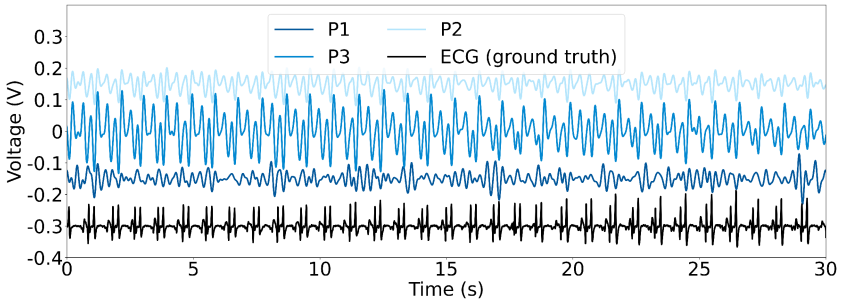

Fig. 9. Time series of the back (P1), left (P2), and right (P3) pressure patches signals along with ECG ground truth. While the user is lying on their back, the side patches capture the pulses stronger than the back patch.

The head posture information during sleep can be useful in understanding which posture leads to better or worse sleep quality. For example, lying on the back is usually not recommended for sleep apnea patients [96]. Figure 8 shows the baseline signal for the P1, P2, and P3 pressure patches when a user is lying in different sleep postures for a total of 15 minutes. As it can be seen, in each sleep posture, the pressed patch has the lowest baseline. This is aligned with our expectation as the voltage being measured via the voltage divider circuit (shown in Figure 11(a)) is inversely proportional to the pressure, so lower voltage means higher pressure.

4.1.3 Respiration and Heart Rate Estimation. In order to accurately estimate respiratory rate from the pressure sensors' baseline signals (an example is shown in Figure 5(b)), we first apply FFT to find the frequency bin with the highest power resulting from the respiration signal. Then, we perform band-pass filtering based on the FFT peak to avoid counting fluctuations of the second harmonic. We then count the number of peaks in one-minute-long windows of the filtered time series to obtain the respiration rate. The estimated respiration rate is updated once every half minute (the step size is 30 seconds). The strongest respiration signal is obtained from the patch on which the head is resting, i.e., the most pressure is sensed.

The estimation of the heart rate is more challenging as the cardiac signal captured by the pressure patches has very low SNR due to the mixed-in involuntary head movements, and the noise in all frequency bins. Furthermore, the amplitude of the cardiac signal can also be affected by many factors including sleep posture and the user's physiological characteristics.

Generally, the signal captured by the patch under pressure in each sleep posture has better resolution in capturing the small head movements related to cardiac activity. An example is shown in Figure 5(a), where the user is lying on their back and the back patch (P1) can clearly capture the heartbeats, better than the other two sensors. However, this assumption does not always hold true. Figure 9 shows another example of when the user is lying on their back and this time, the back pressure signal (P1) is quite corrupted while the right (P3) and left (P2) signals clearly detect the heartbeats. This can happen due to several reasons. Having wrinkles in the pressed patch decreases the sensor sensitivity and results in a poor and noisy signal. Also, for the users who naturally have strong superficial temporal artery pulse on the temple, the heartbeat signals captured from side patches are much stronger than the back patch that only detects the subtle head motion caused by the Newtonian reaction to the influx of blood at each beat. Therefore, we have two main challenges that we need to encounter when designing our algorithm: (1) the heartbeat signal is weak and usually interfered with by many sources of noises, and (2) the signal quality of patches differs across different users and sleep postures. In the following, we describe our proposed heart rate detection algorithm summarized in Figure 10.

In order to block the DC baseline, respiration related frequency components, and higher frequency noises, we apply a 5th order Butterworth filter with a passband of 0.75–3 Hz on three cardiac signals. Please note that a normal adult's resting pulse rate falls within [0.75, 2] Hz, or [45, 120] beats/minute. After eliminating some of

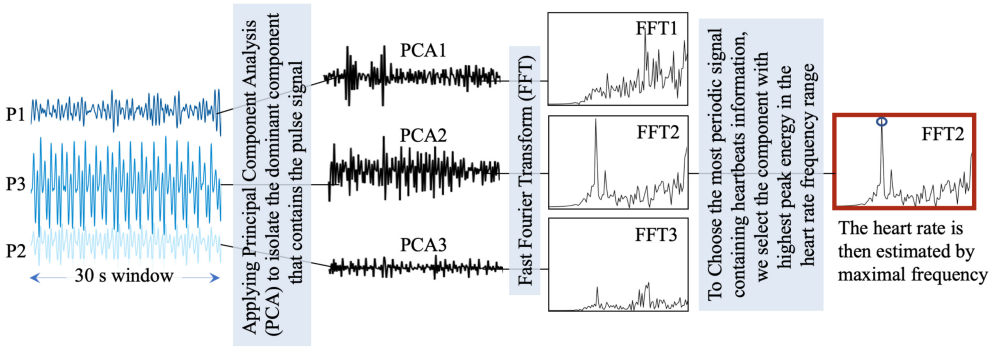

Fig. 10. PhyMask heart rate detection algorithm pipeline.

the noise, we need to isolate the heartbeat component of the three signals. In order to do this, we use **Principal Component Analysis** (**PCA**) to isolate the dominant component that contains the pulse signal. To do this, we consider each pressure patch signal stream as a separate data point and use PCA to find a set of basis vectors along which the signal has the most variation. We then select a dimension on which to project the time series to obtain the pulse signal.

The 3 filtered BCG signals at time t are represented by $m_t = [y1(t), y2(t), y3(t)]$. PCA finds the principal axes of variation of the signal as the eigenvectors of the covariance matrix of the data Σm, i.e.,

$$\Sigma m \, \Phi m = \Phi m \, \Lambda m, \tag{1}$$

where Λm denotes a diagonal matrix of the eigenvalues $\lambda 1$, $\lambda 2$, and $\lambda 3$ corresponding to the eigenvectors in the columns of Φm, $\phi 1$, $\phi 2$, and $\phi 3$. We finally obtain three 1-D signals $si(t)$ by projecting m_t onto ϕi.

$$s_i(t) = \sum_{t}^{T} m_t \phi i. \tag{2}$$

We then select the most periodic component $s_p(t) = \arg\max_{s_i} h(s_i(t))$ for heart rate estimation, where the function $h(.)$ calculates the periodicity of the input signal as the percentage of the spectral power accounted for by the frequency with maximal power to the total spectral power. The heart rate is then estimated as $\frac{60}{f_{pulse}}$ beats/minute, where f_{pulse} is the maximal frequency of $s_p(t)$. Please note that we perform PCA on a 30-second window and slide it with a hop size of 10 seconds.

4.2 PhyMask Hardware and Data Acquisition

We now turn to describe our hardware platform. PhyMask uses a single low-power and compact circuit board for filtering, amplification, digitization, and transmission of the raw EEG, EOG, cardiac, and respiratory signals collected from the biopotential electrodes and the pressure patches. There are three main challenges in designing such a board: first, each of these signals has different characteristics that require specific electronics circuitry design; second, all of the signal channels need to be collected at a high-enough sampling rate and transmitted at the same time to ensure real-time and accurate tracking; third, the board should have very low power consumption enabling long-term usability of the system with a single battery charge. In the following, we explain the steps taken to tackle these challenges in the design of the PhyMask electronics.

As mentioned before, the board is connected to 3 biopotential electrodes (one reference and two sensors) and 3 pressure sensors. The biopotential electrodes provide the EOG and EEG signals while pressure sensors provide cardiorespiratory signals. Our board is composed of three main modules: (1) EEG and EOG signals

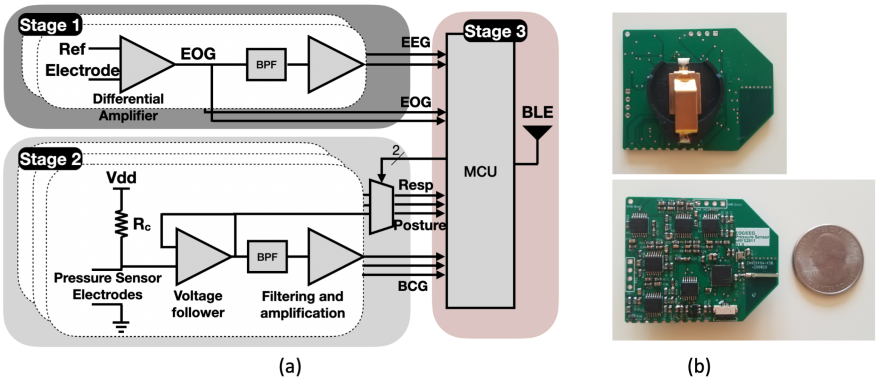

Fig. 11. PhyMask board. (a) Block diagram of the analog circuit board. The board has three main stages responsible for biopotential signals sensing, pressure sensors sensing, and signals transmission. (b) Front and rear view where the battery should be placed.

acquisition, (2) cardiac and respiration signals acquisition, and (3) low-power wireless signal transmission. The board schematic is illustrated in Figure 11(a).

Stage 1: EEG and EOG signals collection. EEG and EOG signals have very different characteristics. EOG signals, representing eye movements, have magnitudes in the orders of 100s of μVs with a frequency range of about DC-100 Hz. EEG signals, however, are roughly three orders of magnitude weaker than the EOG signals, and their frequency content during sleep can vary from 0.5 Hz to about 30 Hz.

To deal with this, we use two two-stage differential amplifiers each amplifying one biopotential signal with respect to the reference electrode. The gain of the first stage is about 30 and it outputs the EOG signal stream. We selected this level of amplification gain empirically such that the obtained EOG signal is clearly distinguishable, yet it does not saturate the next stage amplifier. This diminishes the need for a DC reject filter which consequently would have eliminated critical low-frequency contents of the EOG signal. In the second stage of the amplifier, we further amplify this signal by 2,500 times and filter it to only pass through frequency content in the range of 1–50 Hz to acquire the EEG signal.

Stage 2: BCG and respirations signals collection. As discussed earlier, the fabric-based pressure patches are designed to capture the subtle ballistics and head movements caused by cardiorespiratory activities. But these two signals are very different—the pressure response of respiration is stronger than the heartbeat, and the respiration signal contains very low-frequency components (typically, below 1 Hz) whereas the cardiac signal is in the 1–20 Hz frequency range.

The second stage of the board receives the signal from three pressure sensors and after using a voltage divider to translate resistance changes into changes in voltage, we use a voltage follower to create a copy of the signal with low output impedance for each channel, suitable for digitization. The resultant three signals represent the posture/respiration signals of the user. To find the heartbeat instances in these signals, we then DC reject and amplify the signals up to 400 times to find the ballistics of the veins covered by the sensor.

Stage 3: low-power wireless signal transmission. The last module of the board uses a low-power MCU with integrated BLE capability (nRF52811 [16]) to wirelessly transmit the acquired data to the host device. The MCU is capable of converting a maximum of 8 simultaneous analog channels into digital signals. This is less than the 10 analog channels captured by PhyMask, i.e., 2 EEG, 2 EOG, 3 cardiac, and 3 respiration. A naive solution would be to sequentially sample each channel and effectively reduce the sampling rate of all channels symmetrically. However, given the fact that the dominant frequency content of respiration is placed lower in frequency spectrum compared to other desired signals, we placed a 3:1 analog MUX to output one of the three respiration signals in each sampling round. As a result, the effective sampling rate of the respiration

signal is one-third of the other physiological signals. The decisions presented above result in a sampling rate of 125 samples per second for EEG, EOG, and cardiac signals, while providing 42 samples per second for the respiration signal. These sampling rates are sufficient for the reconstruction of the above signals given the fact that EEG, which contains the highest frequency content among all, requires a minimum sampling rate of 60 Hz to reach the Nyquist rate and the respiration signal requires a minimum sampling rate of 2 Hz.

Our choice of sampling rate is also limited by power consumption and hardware compatibility considerations. A higher sampling rate leads to a higher transmission rate for the BLE module which greatly increases the power consumption; on the other hand, some host devices have lower bound restrictions for transmission interval in their BLE connection. In our setup, the transmission interval is set to 100 ms which makes the system capable of connecting with devices with more strict restrictions and leads to the average power consumption of 3.3 mw. The power consumption of the analog processing components and the MUX is negligible in comparison with the MCU. This means that with a small battery of 250 mAh, 250/1.1 capacity, PhyMask can run up to 5 days. An image of the board, which has dimensions as small as 4 cm by 5 cm, is presented in Figure 11(b).

Once signals are captured and transmitted to the host device, we apply notch, median, and outlier filters in order to remove the powerline noise and smooth out the signals. Then we filter each signal with a tailored band-pass Butterworth filter (we choose 5th order for its maximally flat passband). Examples of the PhyMask collected EEG, EOG, BCG, and respiration signals are shown in Figure 5.

5 DATASET COLLECTION AND LABELING

In this section, we explain the details of our user study and the ground truth labeling approach. All of these datasets were collected under Institutional Review Board approval.

5.1 Benchmarking Dataset

Our first data collection aims at evaluating PhyMask's ability in detecting heart rate, respiration, sleep posture, gross body movement, and eye movement. For this, we asked 10 participants (average age of 27) to wear PhyMask and we recorded the output voltage in various stationary conditions. Participants varied in weight, 110–220 lb, and height, 5'1"–6' . 4 out of 10 participants were females.

We asked our participants to lie down on their back, left, and right sides, posing a sleep position that feels natural to them. We collected data for five minutes in each sleep posture. Then we demonstrated to the participants a set of both smooth and jerky limb movements that are common during sleep (particularly for sleep disorders like periodic limb movement). We then repeated the first experiment and asked our participants to mimic these movements while in the sleep positions. The participants were also asked to perform random eye movements in each position for two minutes. The whole experiment led to a total of ∼30 minutes of recording from each user. Each recording consists of ten channels, six of which correspond to pressure sensing patches and four corresponding to the hydrogel fabric electrodes.

5.2 Nap Dataset

Our second data collection aims at validating PhyMask's ability in gross-body movement, sleep micro-events, and sleep stage detection in a naturalistic nap setting across five participants (4 males and 1 female). The participants were asked to wear PhyMask while sleeping for about two hours in the University of Massachusetts sleep lab facility. We collected a total of 504 minutes of nap data. Please note that the users were given no specific instructions regarding how to sleep, so they were free to choose their own posture and change it as they wished.

5.3 Sleep Dataset

Our third data collection aims at validating PhyMask's ability in measuring the brain electrical activities EEG and microsleep events in a more uncontrolled setting over a long time of wear. For this, we asked a participant

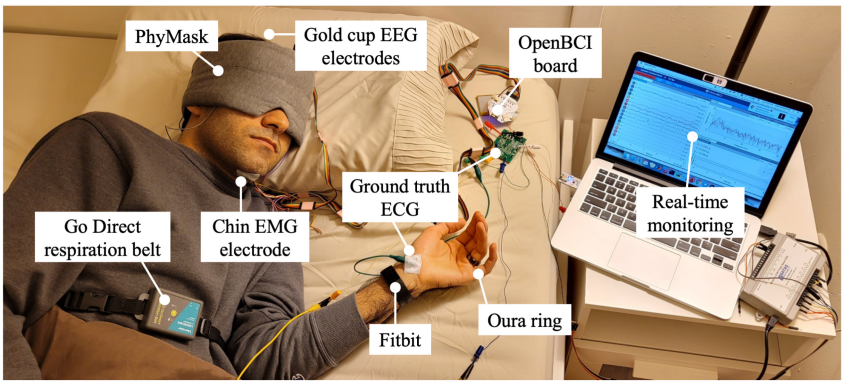

Fig. 12. Data collection setup.

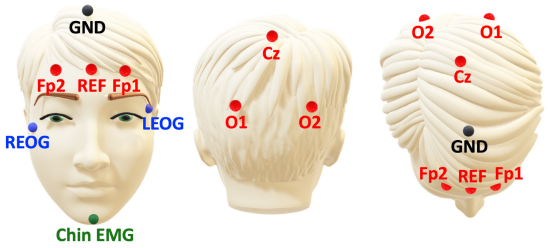

Fig. 13. The ground truth gold-cup electrodes' placements used in our sleep monitoring study, based on the standard 10–20 EEG recording system.

(male) to wear PhyMask for five night sleep sessions and we collected the signals for a total of 2,118 minutes (about 7 hours per night). Due to the COVID-19 precaution, the experiment took place in participant's home, providing him a safe environment to perform the study. In addition, it allowed us to collect more naturalistic sleep behavior.

To evaluate how PhyMask compares to commercially-available sleep tracking wearables, we asked our participants to wear a Fitbit Charge 2 and an Oura Ring (fit size 11). The Fitbit and Oura Ring are the dominant sleep tracking wearables in the market, and this comparison allows us to gauge the benefits that PhyMask can provide due to measuring the EEG signal in addition to the physiological signals collected by these wearables.

5.4 Ground Truth Annotation

For ground truth, the PSG data were collected simultaneously with data from PhyMask. PSG included electroencephalographic (EEG: Fp1, Fp2, Cz, O1, O2 sites), chin EMG, and EOG recordings performed according to **American Academy of Sleep Medicine** (**AASM**) rules [1] (the electrodes placement is shown in Figure 13). The electroconductive paste (Ten20 [8]) were used to improve contact between the participant's scalp and the gold cup electrodes (with 10 mm diameter [5]). In order to synchronize PhyMask's EEG signals with the eight channels of the ground truth data, the two sets of signals were collected via the same board. For the nap study, we used the Embletta MPR sleep system [12], with a sampling rate of 500 Hz. For the night sleep study, we used an OpenBCI Cyton amplifier [2] and the expansion Daisy Module [2], with a sampling rate of 125 Hz. The OpenBCI board was wirelessly connected to a laptop by the USB Dongle.

We also collect ground truth measures of the target physiological signals. For heart rate, we use a three-channel ECG measurement (2 wrists and an ankle) using the AD8232 evaluation board [7] (sampling rate of 200 Hz), and

for respiration, we used a Go Direct respiration belt [4] (sampling rate of 10 Hz). Figure 12 shows a user sleeping while wearing PhyMask, sleep tracking wearables, and all the ground truth devices.

Sleep stages (Wake, N1, N2, N3, REM sleep) were scored in 30-second epochs by certified sleep experts according to sleep scoring guidelines of AASM [32], separately for both PSG and PhyMask. In addition, the sleep micro-events i.e., spindles and K-complexes, were annotated (2,094 number of spindles and 1,397 number of K-complexes in the sleep dataset, and 470 number of spindles and 217 number of K-complexes in the nap dataset). For this, a sleep specialist first mark the events with Embla RemLogic PSG software [3], and then visually validate all the events.

6 EVALUATION

In order to evaluate PhyMask, we break down the results into two subsections. In Section 6.1, we analyze the performance of our hydrogel electrodes in picking up the brain activity and eye movement signals. We present PhyMask results in detecting sleep stages as well as sleep micro-events (spindle and K-complex), and compare it with commercial wearable trackers. In Section 6.2, we evaluate our pressure patches performance in estimating the head posture, gross body activity, and respiration and heart rate in various sleep postures.

6.1 Evaluation of Hydrogel Electrodes in Measuring Biopotential Signals

In this section, we explore our novel fabric hydrogel sensor's ability in measuring brain waves and eye movement patterns during the longitudinal sleep study. To the best of our knowledge, this is the first time to measure EEG with all-fabric sensing elements during sleep. The validation of this sensor can potentially impact the next generation of EEG monitoring wearable devices.

6.1.1 Evaluating PhyMask Signal Integrity. We start by evaluating the quality of the biopotential signals (i.e., EOG and EEG) obtained from the textile electrodes.

We evaluate EOG signal quality using the **Zero-Normalized Cross-Correlation** (**ZNCC**) metric. We report the ZNCC score between the signal captured by our hydrogel electrodes and the gold cup electrodes placed at the standard location, i.e., HG1 with LEOG and HG2 with REOG (The sensor placement is shown in Figure 13). We first apply a 5th order Butterworth filter with a passband of 0.1–20 Hz, and then calculate ZNCC score as defined by the following formula

$$ZNCC = \frac{1}{n} \sum_{x} \frac{1}{\sigma_f \sigma_t} (f(x) - \mu_f)(t(x) - \mu_t), \tag{3}$$

where n is the length of $f(x)$ and $t(x)$, μ_f is the average of f, and σ_f is the standard deviation of f.

Figure 14(a) illustrates the ZNCC score of 10 participants for lying back, right, and left scenarios (benchmarking dataset). As can be seen, the results are consistently good under different postures. This shows that the hydrogel electrodes precisely capture the low-frequency content of the EOG signal even when there is inconsistent pressure applied on the hydrogel electrodes caused by various sleep postures. We observe that the inconsistent pressure only affects the baseline which is removed by our band-pass filter. For the nap and sleep datasets, we calculate the ZNCC score only during the N1 and REM sleep stages, in which the slow-rolling and rapid eye movement events happen, respectively. The results are summarized in Figure 14(b) and (c). The results show a strong correlation between our textile electrodes and the ground truth gold cup electrodes even in an uncontrolled setting where the participants could freely move during sleep.

We evaluate the EEG signal quality using the coherence measure. This metric is known to identify the level of coupling in cortical pathways given its sensitivity to signal phase difference. Maximum coherence occurs when the phase difference is fixed between two signals and a near zero coherence value indicates a random phase

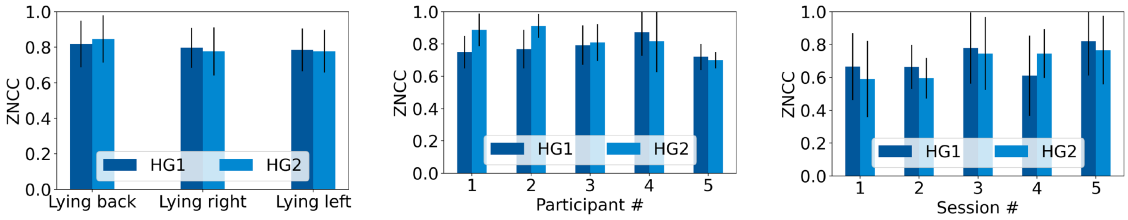

(a) Benchmarking dataset (b) Nap dataset (c) Sleep dataset

Fig. 14. ZNCC values for the electrode pairs, HG1/Fp1, and HG2/Fp2. For the benchmarking dataset, the results are averaged across all 10 participants for different sleep postures. For the nap and sleep datasets, we calculate the ZNCC measure over the sleep stages that include the most eye movement events (i.e., N1 and REM).

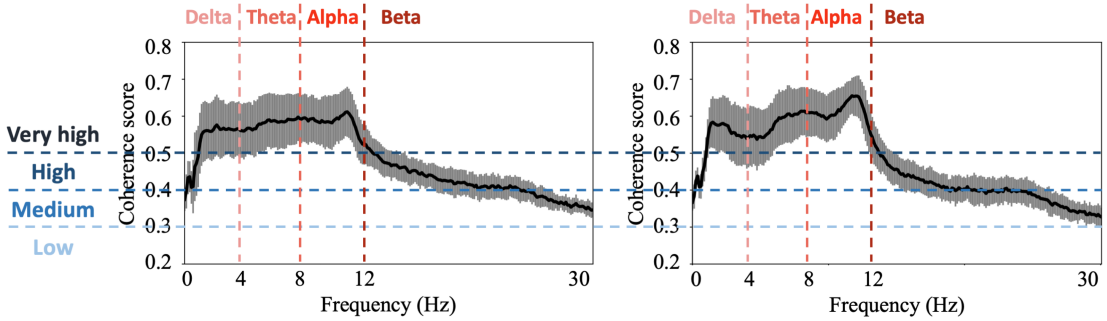

(a) Right side (Fp2 and HG2) (b) Left side (Fp1 and HG1)

Fig. 15. The averaged coherence measures over each frequency domain is illustrated for two groups of signals.

difference between signals over time [47, 111]. Coherence is calculated as

$$C_{xy}(f) = \frac{|\, G_{xy}(f)\,|^2}{G_{xx}(f)\, G_{yy}(f)}, \tag{4}$$

where $G_{xy}(f)$ is the Cross-spectral density between x and y, and $G_{xx}(f)$ is the auto spectral density of x.

The goal is to evaluate how precisely our electrodes can pick up the brain signals with respect to the gold standard EEG recording approach used in PSG, in an uncontrolled and naturalistic setting over a long time of sleep. We calculate the coherence metric for the signal captured by our hydrogel electrodes and the gold cup electrodes placed at the nearest standard location, i.e., HG1 with Fp1 and HG2 with Fp2, over 30-second epochs in the frequency domain for more than 35 hours of sleep data.

Figure 15 illustrates the averaged coherence measures over each frequency domain. As suggested by previous studies in EEG signal analysis [47], we label the coherence scores as follows: low (0.2–0.3), medium (0.3–0.4), high (0.4–0.5), and very high (0.5–1). As it can be seen, the majority of frequency domains have very high coherence scores, confirming the maximum coupling between our fabric-based hydrogel electrodes and the standard gold-cup electrodes. Please note that for analysis of EEG signal during sleep, we are more interested in the Delta (0.5–4 Hz), Theta (4–7 Hz), and Alpha (8–12 Hz) sub-bands, as the Beta (12–25 Hz) is present when the person is awake with open eyes and is actively thinking [100].

While Figure 15 illustrates very high coherence for the two groups of signals, it is also important to understand whether the coupling changes as time progresses. In order to investigate this factor, we have plotted the coherence score of the HG2/Fp2 pair for two different full-night sleep sessions in Figure 16. For night #1, the

Table 3. Analysis of Average Coherence Measure between HG1/Fp1 and HG2/Fp2 Over Frequency Band (0.5–25 Hz) under Different PhyMask Shift Scenarios

No shift	Horizontal shift 2 cm	Horizontal shift 1 cm	Vertical shift 1 cm up	Vertical shift 1 cm down
0.53	0.46	0.41	0.55	0.35

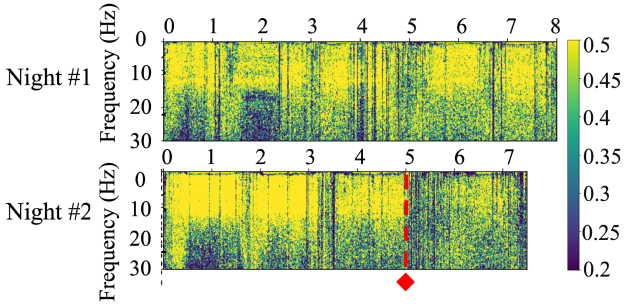

Fig. 16. Time series of the coherence score of the right hydrogel electrode/Fp2 pair for two different nights. While the coherence is consistently high for night #1, for night #2, it degrades after 5:00 due to sudden body motions.

consistently high coherence score (above 0.4) in the lower frequency band (0.5–12 Hz), which includes Delta, Theta, and Alpha waves, indicates good performance and high coupling between HG2 electrode and standard Fp2 electrode. However, for night #2, the coherence degrades after time 5:00 (marked with a red arrow). The reason for this observation is that during that time interval, the user had sudden body movements and roll-overs that resulted in PhyMask's displacement (about 2 cm shift to the right). We see that even with this level of displacement, the average coherence measure is around 0.4 which is well within the acceptable range [47].

In order to quantify the effect of the PhyMask displacement on the coupling between the hydrogel electrode (HGx) and their corresponding standard electrode (Fpx), we conduct a new experiment in which we asked a participant to sleep in the supine position and we shifted the PhyMask in 4 different placements (1 cm left, 2 cm left, 1 cm up, and 1 cm down). We collected 10 minutes of data in each setting. Table 3 shows the average coherence measure for both electrode pairs over the frequency band (0.5–25 Hz). As it can be seen, the further horizontal shifts result in lower coherence measure, as the captured signal by the PhyMask differs more from the standard (Fpx) signal by an increase in the distance. With regards to the vertical shift, the coherence measure increases when the PhyMask moves closer to the standard electrode locations (1 cm up shift). On the other hand, a 1 cm down shift results in the lowest coherence. We figured that is because in this case, the hydrogel electrodes touch the eyebrows which leads to poor skin-electrode impedance and hence degradation in the coherence. Please note that the degradation in the coupling of the signals due to the PhyMask shift does not essentially lead to the degradation in the overall performance of PhyMask. Although the captured signals by PhyMask would be different from the EEG signals captured from standard Fpx location, they still contain the EEG frequency spectrum information needed for sleep stage monitoring. As shown in [49, 85], the sleep stages information can even be extracted from a single-channel EEG, as long as the electrode maintains good contact with skin.

6.1.2 Sleep Spindle and K-complex Detection. In this section, we evaluate (1) how well PhyMask is able to detect spindles and K-complexes, and (2) how PhyMask compares to PSG-based spindle and K-complex detection; PSG has higher-dimension EEG signals captured by standard electrodes from various points on the scalp, so it provides a measure of the best-case performance.

In order to compare the performance of PhyMask with PSG in sleep micro-event detection, we train our classifiers explained in Section 4.1.1 separately on PhyMask EEG data and the gold standard PSG. The results

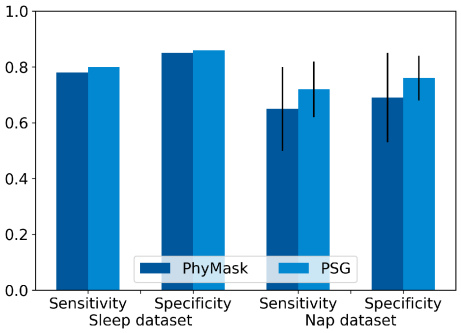

Fig. 17. Comparing spindle detection of PhyMask versus PSG.

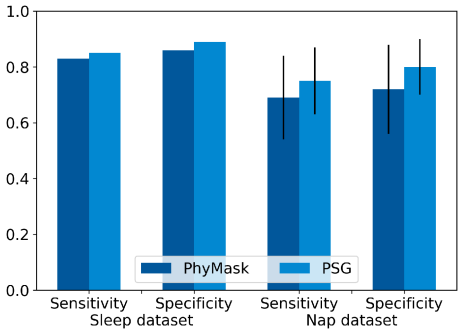

Fig. 18. Comparing K-complex detection of PhyMask versus PSG.

of the binary classifiers for spindle and k-complex detection are summarized in Figures 17 and 18, respectively. For the sleep dataset, we trained our classifiers on the first three nights and used the fourth and fifth nights as the validation and the test set, respectively. For the nap dataset, we use the **leave-one-subject-out** (**LOSO**) validation approach. Due to the highly imbalanced nature of the data, we use sensitivity and specificity measures for evaluating the performance of the micro-event detectors as also common in the literature [95, 102].

$$Sensitivity = \frac{TP}{TP + FN} \qquad Specificity = \frac{TN}{TN + FP}. \tag{5}$$

Our results are very promising and show that PhyMask accurately detects spindle and K-complex events with an average median of higher than 0.73 sensitivity and 0.78 specificity scores. This means that PhyMask is capable of recording high fidelity EEG signals that contain micro-sleep events such as spindles and k-complexes. As it can be seen, the results of the nap study slightly degrade compared to the sleep study. We believe that in the future, we can address this challenge and make the model more robust and generalizable across various users, by personalizing our model with enough datasets and using more complicated structures such as CNN/RNN. We talk more about this in Section 7.

6.1.3 Validation of PhyMask Against Polysomnography for Sleep Stage Tracking. In this section, we evaluate the quality of the PhyMask signal against gold-standard PSG for the purpose of sleep stage tracking. In order to do this, the PhyMask and PSG data from both nap (≈10 hours) and sleep (≈35 hours) datasets have been annotated by sleep experts into five sleep stages, i.e., N1, N2, N3 (Deep sleep), REM, and Awake. Due to the low number of N1 stage instances in our dataset, we grouped both N1 and N2 stages as Light sleep. In order to quantify the level of agreement for annotated sleep stages between PhyMask and PSG, we use Cohen's kappa [38] defined as follows:

$$\kappa = \frac{p_o - p_e}{1 - p_e}, \tag{6}$$

where p_o is the relative observed agreement among raters, and p_e is the hypothetical probability of chance agreement, using the observed data to calculate the probabilities of each observer randomly seeing each category. If the raters are in complete agreement then $\kappa = 1$. If there is no agreement among the raters, $\kappa = 0$. It is possible for the statistic to be negative, which implies that there is no effective agreement between the two raters or the agreement is worse than random.

It is well-known that there exists inevitable variability and disagreements between human experts on epoch ratings—Wang et al. [114] found kappas of 0.72–0.85 between two human raters and kappas of 0.82–0.85 between well-performing raters. Therefore, a Cohen's kappa of 0.8 is considered to show strong agreement once we take into account such variabilities. The Cohen's kappa coefficients for each sleep stage are illustrated in Figure 19.

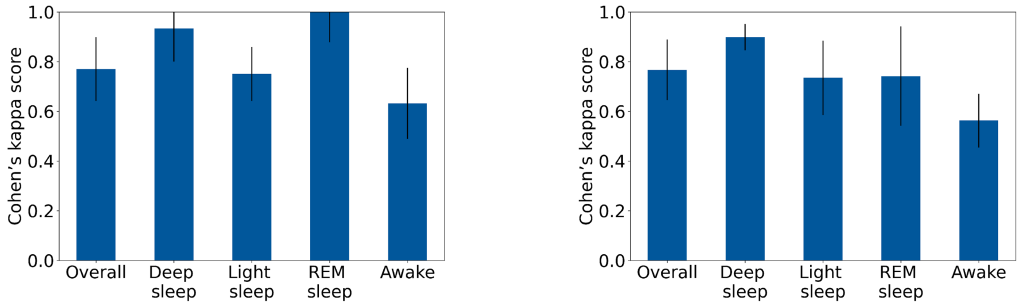

(a) Nap dataset: median cohen's kappa measures over all five participants.

(b) Sleep dataset: median cohen's kappa measures over all five sleep sessions.

Fig. 19. The agreement between standard PSG and the PhyMask sleep stages scores is validated with Cohen's kappa metric for each sleep stage.

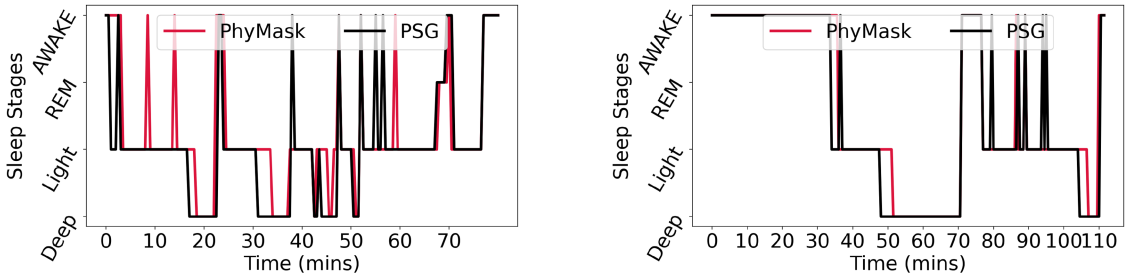

(a) Participant #1

(b) Participant #2

Fig. 20. The extracted sleep stages from ground truth (PSG) and PhyMask for the the nap study.

For the nap dataset, the coefficients are calculated over the five participants (total number of epochs = 1,140), and for the sleep dataset, the coefficients are calculated overall five sleep sessions (total number of epochs = 4,236). The overall performance of PhyMask reaches the state of the art with a median Cohen's kappa of 0.77. For most of the sleep stages, PhyMask agrees very well with the PSG. This high level of agreement between PhyMask and PSG further validates the quality of the measured EEG signal and shows that PhyMask successfully captures information that is critical for sleep stage tracking.

There is a gap in the Cohen's Kappa score of the REM sleep stage between the nap and sleep datasets. This is because the nap dataset only contains 7 epochs of the REM stage, while there are 742 REM stage epochs in the sleep dataset. This indicates that the majority of our participants could not reach the REM stage and complete the sleep cycle during the short time period of their nap. This observation is aligned with our knowledge of the REM sleep stage. As it is explained by Carskadon et al. [33], stage REM occurs about 80–100 minutes after you fall asleep, and lasts roughly 10 minutes the first time, increasing with each REM cycle. Figure 20 illustrates the examples of sleep stages captured by PhyMask and the gold standard PSG for two participants. As it can be seen, only participant #2 stayed in the REM stage for a very short time period.

The common misclassified stage in PhyMask data is Awake. In order to better understand when sleep stage misclassifications happen, we calculate the confusion matrix (Figure 21), each data point in the confusion matrix represents a 30-second epoch. As can be seen, the awake stage is mostly confused with the REM stage. Since, these stages have overlapping frequency bands (13 Hz–30 Hz), the main distinguishing signal between the two is

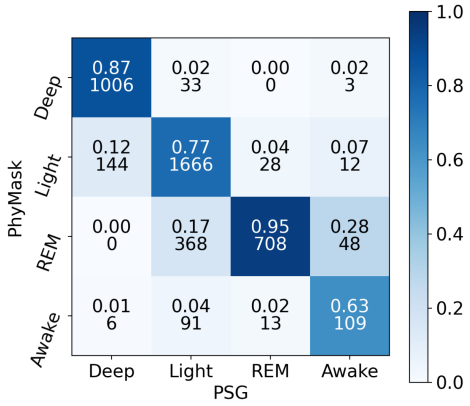

Fig. 21. The confusion matrix of PhyMask in sleep stage classification.

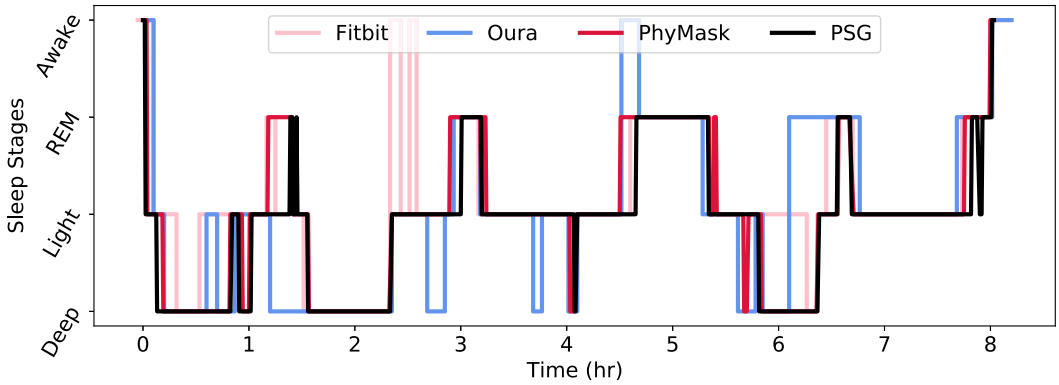

Fig. 22. The extracted sleep stages of one full-night sleep for ground truth (PSG), PhyMask, Oura, and Fitbit.

the EOG. During the REM stage, as its name suggests, fast rapid eye movements occur as opposed to slow rolling eye patterns that happen during the Awake/drowsiness stage [97]. PhyMask can only capture the horizontal eye movements; however, human raters are trained on conventional data that includes both horizontal and vertical eye movement patterns. We believe that this might have led to lower classification accuracy in this case, and we hypothesize that in the future, training a classifier on the PhyMask data should significantly help with this.

6.1.4 Comparison between PhyMask and Commercial Sleep Trackers. In this section, we compare PhyMask with two other commercially-available sleep stage tracking devices i.e., Fitbit Charge 2 and Oura Ring. For this section, we only consider the sleep dataset and do not include our nap dataset. This is because Fitbit could not detect sleep episodes shorter than 3 hours as stated by their website [13]. Furthermore, the Oura ring that we used for sleep data (size 11) did not fit the majority of our participants in the nap study and hence could not provide reliable information. Figure 22 illustrates the extracted sleep stages of one night from the three devices with respect to the PSG groundtruth system.

We compare the accuracy, precision, recall, and f1 score measures of PhyMask, Oura, and Fitbit, calculated as

$$Accuracy = \frac{TP + TN}{TP + TN + FP + FN} \quad Precision = \frac{TP}{TP + FP} \quad Recall = \frac{TP}{TP + FN} \quad F1\ score = \frac{2TP}{2TP + FP + FN}, \tag{7}$$

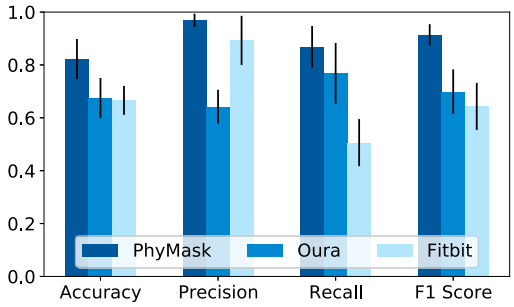

Fig. 23. Accuracy, precision, recall, and F1 score of sleep staging for five sleep sessions overall of the sleep stage categories.

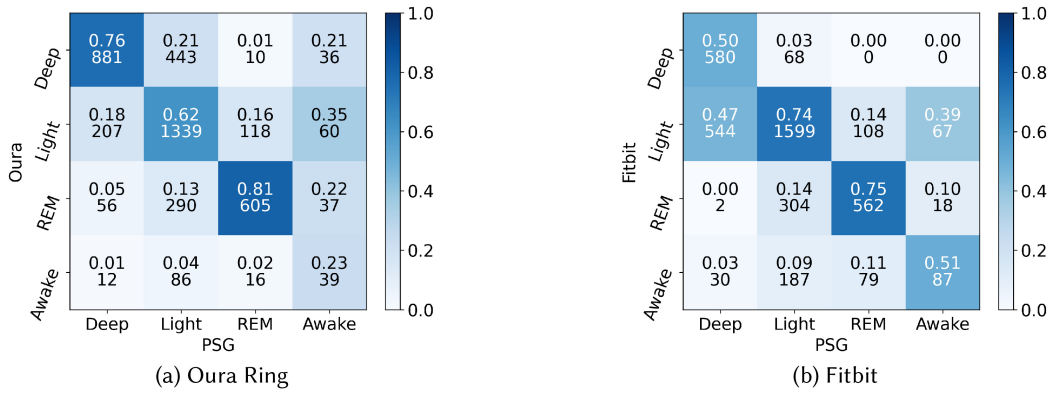

Fig. 24. Sleep stage classification results: the confusion matrices show the performance of Oura and Fitbit.

where **true positive** (**TP**) is the number of actual positive epochs which are correctly classified; TN (true negative) is the number of actual negative epochs which are correctly classified; FP (false positive) is the number of actual negative epochs which are incorrectly classified as positive; FN (false negative) is the number of actual positive epochs which are incorrectly classified as negative.

Figure 23 summarizes the results for all of the sleep stages overall nights data. PhyMask outperforms the other two devices in terms of all four metrics, which demonstrates the advantage that PhyMask offers in accurate sleep stage tracking by leveraging its capability in recording the EEG signal.

We also calculate cohen's kappa measures and confusion matrices for Oura and Fitbit (Figure 24). Oura (median kappa = 0.54) and Fitbit (median kappa = 0.51) have much lower kappas than PhyMask (median kappa = 0.77). The low accuracy of these sleep trackers in detecting sleep stages has also been observed by previous studies [36, 42, 43]. Since we do not have access to the raw data captured by Oura and Fitbit sleep tracking algorithms, we cannot fully analyze their behavior. However, if we look at the confusion matrices, we find that Oura has a very low recall for the Awake stage. This is because Oura does not provide the micro-awake events after sleep onset in their provided sleep hypnogram on the dashboard. They instead seem to be reported as the closest sleep stage and that is why the predicted labels for Awake events by Oura are distributed almost evenly among all the stages. Fitbit, on the other hand, has a noticeable bias towards classifying sleep sessions as the Light sleep stage. Figure 24(b) shows that nearly half of the Deep sleep stage epochs are wrongly classified as Light stage. This is an example where leveraging the EEG signal can greatly boost the performance as these two stages can easily be differentiated based on their frequency content (Deep: 0.5–4 Hz and Light: 4–8 Hz).

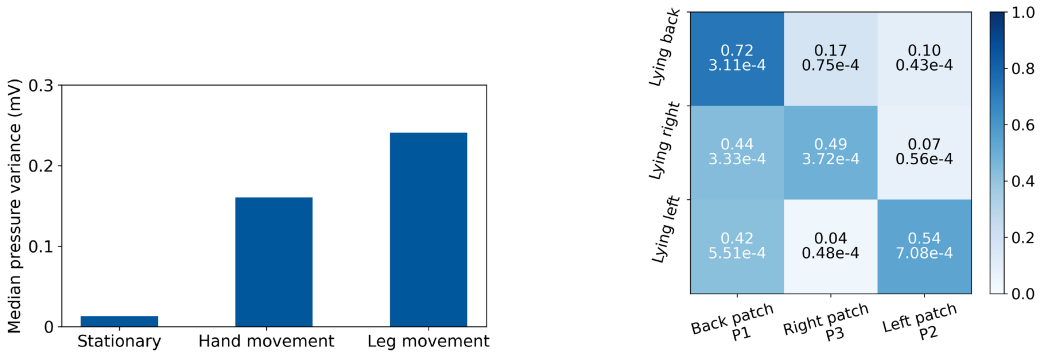

(a) The median variance of baseline signal voltage of the pressure patches for stationary, hand movement, and leg movement scenarios across all sleep postures and participants.

(b) The median variance of each patch baseline voltage during limb movement periods over each sleep posture across all participants.

Fig. 25. Analysis of baseline voltage changes of the pressure patches for limb movement scenarios in different sleep postures. We can see that pressure patches easily capture information on gross body movement.

6.2 Evaluation of Pressure Patches in Measuring Physiological Parameters

In this section, we evaluate the performance of our novel pressure-based method for detecting the physiological variables of interest. For this purpose, we use our benchmarking dataset in Section 5.1.

6.2.1 Head Posture and Gross Body Movement Estimation.

Gross body movement. As discussed earlier, the PhyMask pressure patches are designed to be sensitive to capture the subtle head movements caused by heart pulses and respiration. Therefore, gross body movement, which is an important marker for sleep tracking and sleep disorder diagnosis, can easily be detected by the embedded pressure sensors.

In order to evaluate this, we asked our participants to mimic both smooth and jerky limb movements that are common during sleep in each sleep posture (Section 5.1). The median variance of baseline signal voltage of the three patches for stationary, hand movement, and leg movement scenarios across all sleep postures and over 10 participants are illustrated in Figure 25(a). As can be seen, the variance difference between the limb movement scenarios and the stationary scenario is very distinct. We can also see that the signal corresponding to the hand movement scenario has lower variance compared to the leg movement scenario since people in general use more force to move their legs as opposed to their hands due to the legs physical characteristics such as weight and length which results in applying more pressure on the patches. As a result, even naive thresholding on the variance of the pressure patch signals can identify different types of gross body movement events.

In order to understand how gross motor activity affects each pressure patch in different sleep postures, we calculate the variance of each patch baseline voltage during limb movement periods over each sleep posture. The median voltage across all participants is shown in Figure 25(b). As can be seen, the under-pressure patch has the highest variance meaning the higher sensitivity to detect the body movements. An interesting point is that in both lying on the right and left scenarios, the variance of the back patch is as high as the pressed patch. This is because, based on our observation, the participants tend to swing their whole body a bit back and forth while doing the activities, specifically during the leg movements. These motions greatly affect the back patch which results in high variance.

To understand how pressure patches can pick up the natural limb and body movements during sleep, we analyze the data from our five participants in the nap study Section 5.2. For the ground truth, we use a gyroscope sensor embedded in the Embletta data acquisition unit around the waist area and two EMG sensors attached to

Table 4. PhyMask Performance in Gross Body Movement Detection

Participant	True positive	False positive	False negative
1	4	2	1
2	5	2	2
3	3	1	0
4	5	1	1
5	4	2	1

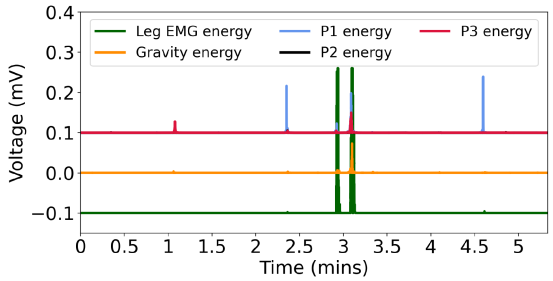

Fig. 26. Time series of the body movement events while the participant is sleeping. The energy of the ground truth (gyroscope and leg EMG) and the PhyMask pressure sensor signals are plotted. There are two head movement events at time indices around 2.4 minutes and 4.6 minutes that are not picked by our ground truth sensors.

the Tibialis anterior muscles of both legs. We annotate the body movement events by applying a threshold over the gyroscope and the legs' EMG energy signals. In order to detect the body movement events from the pressure patches' baseline signals, we first apply a 5th order Butterworth filter with a cutoff frequency of 0.1 Hz. Then we calculate the average energy signals and apply a threshold of 0.05 mV (chosen based on Figure 25(a)) to separate out the gross body movement events. Due to the limited number of body movement events during the short session of nap, we summarized the actual number of true positives, false positives, and false negatives for all the participants in Table 4. The results are very promising showing a relatively high number of true positives. It is interesting to see that the number of false positives is slightly higher than the false negatives. Our hypothesis is that since both of our ground truth sensors (gyroscope and leg EMG) are distant from the head, they cannot pick up the events when the user is adjusting their head on the pillow. The reverse is also true that the pressure patches would not be able to detect small leg movements, however, the threshold is tuned to only consider the gross body movement events. An example of these events is illustrated in Figure 26. As it can be seen, there are two head movement events at time indices around 2.4 minutes and 4.6 minutes that are not picked by our ground truth sensors.

Head posture. In addition to gross motor activity, PhyMask can also provide information about head posture. This information can be useful in understanding which posture leads to better or worse sleep. Head posture can be unambiguously estimated using PhyMask by using the signal baseline across pressure patches (shown in Figure 8). Figure 27 summarizes the voltage changes averaged across all participants for each sleep posture. In each posture, the voltage change is calculated for all the patches (back, right, and left) with the following formula,

$$\Delta V_p = V^s_{p0} - V_p, \tag{8}$$

where V^s_{p0} is the mean baseline voltage of patch p when the participant is in a seated position and there is no pressure applied to the pressure patch, and V_p represents the mean baseline voltage of patch p in the specified sleep posture.

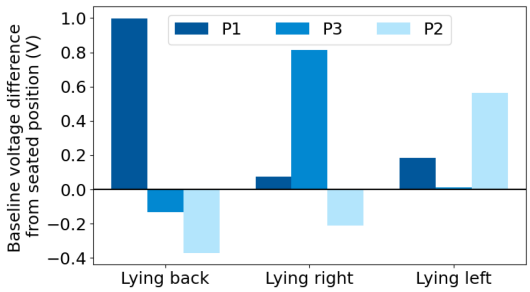

Fig. 27. The mean pressure patches voltage changes across all participants for each sleep posture.

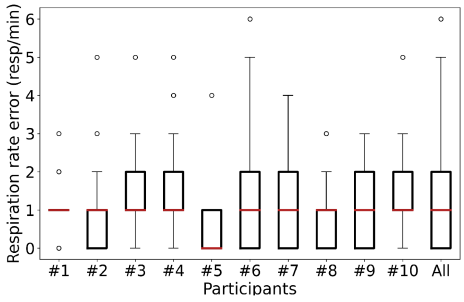

Fig. 28. Performance of PhyMask in estimating breathing rate across all participants.

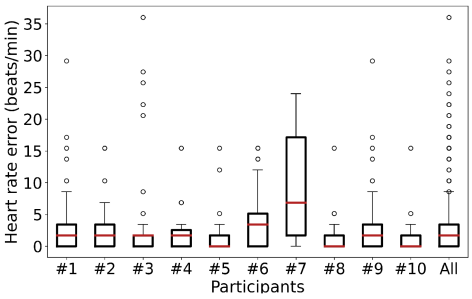

Fig. 29. Performance of PhyMask in estimating heart rate across all participants.

As expected, the pressed pressure patch in each sleep posture has the highest voltage difference compared with other pressure patches. We find that a simple decision tree can easily identify posture with 100% accuracy across all subjects.

Note that the negative voltage occurs when the pressure applied to the corresponding patch in a specific sleep posture is lower than what it is in the seated position. One example is the right and left patches in the *lying on back* sleep posture (Figure 27). This is quite intuitive since in the seated position the right and left pressure patches are resting on the ears and more pressure is applied to them compared to when the person is lying on the back and the side patches are sort of loose.

6.2.2 Respiration Rate Estimation. Figure 28 shows the performance of PhyMask in estimating the breathing rate for all of the participants across three sleep postures. We see that respiration can be accurately captured by the PhyMask pressure sensor simply by looking at periodic pressure changes on the head. The respiration metrics are very good and the median error is generally about 1 resp/minute.

6.2.3 Heart Rate Estimation. The heart rate estimation error is also very good. As can be seen in Figure 29, the median heart rate error overall participants across all the sleep postures is about 1.7 beats/minute, which is within the acceptable error margin (= 5 bpm) for heart rate measurement [50]. The only participant with high error is #7. Based on the ground truth values, we find that this participant has generally weaker heartbeats that result in more subtle head oscillations. We believe that in the future, we can further increase the sensitivity of our pressure patches in order to better detect these small movements. In Section 7, we share some of our thoughts on how we can achieve this.

In Figure 30, we break down the PhyMask performance in estimating heart rate for different sleep postures across all the participants. The results are very promising and show that PhyMask is robust in all the scenarios.

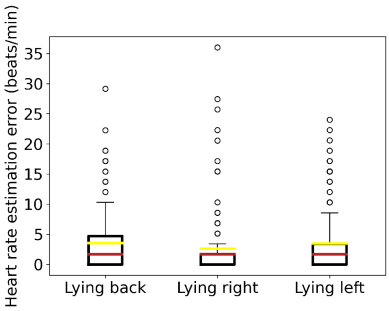

Fig. 30. Performance of PhyMask in estimating heart rate in different sleep postures across all participants.

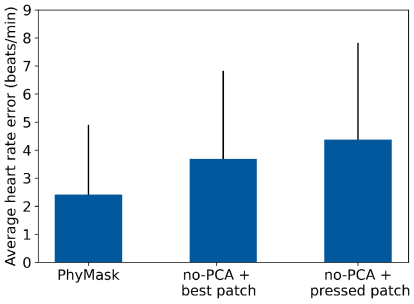

Fig. 31. Comparing the contributions of PCA and best component detection steps in overall heart rate estimation performance.

Breaking down the contributions of the heart rate estimation model components. As described in Section 4.1.3, in order to measure heart rate, we first apply PCA on three pressure patches and then detect the best component that holds the majority of the frequency content corresponding to the heart rate. But one question is how much each of these steps contributes to the overall heart rate estimation performance. To understand this, we compare three variants of our model. First, we have the full model, PhyMask. For the second model, "no-PCA + best patch", we remove the PCA step that is responsible for decomposing the patch signals into sub-signals in order to isolate the pulse. Therefore, the best component detection algorithm is directly applied to the pressure patches, and hence the heart rate is derived from the best-selected patch. Lastly, we look at the performance, when we directly choose the highest peak in the pressed pressure patch derived fft as the estimated heart rate. This model can help us better understand whether the pressed patch is the best patch for accurate heart rate estimation and how effective our best component detection algorithm is. We call this model "no-PCA + pressed patch".

Figure 31 summarizes the results. We see that removing PCA ("no-PCA + best patch") increases the mean heart rate error by about 1.3 beats/minute. This demonstrates that PCA is successful in isolating heartbeats across the three patches. In the case of "no-PCA + pressed patch", where we also remove the best component detection step and directly measure the heart rate from the pressed pressure patch, the mean heart rate error increases about 1 beat/minute. This validates that the under-pressure patch in each sleep posture is not necessarily the most sensitive one. This is also consistent with our observation as described in Section 4.1.3.

6.3 Comfort of Wear

At the end of our user study, we asked our participants to fill out a questionnaire regarding the PhyMask comfort and their preferences. The questions and the users' answers are presented in Figure 32. The results show that the majority found PhyMask quite comfortable. 9/10 users were interested in tracking their physiological signals during sleep. None of the users had used sleep masks before, while 6/10 users had been using wearable tracking devices on a daily basis. While all the participants preferred PhyMask over PSG, only three participants preferred PhyMask over Fitbit/Oura, none of whom owned any wearable tracking devices.

While our sample size is too small to make general conclusions about the above results, we have two hypotheses. For individuals who had not used smartwatches during sleep, the idea of a clothing-based sensor was appealing. Hence three of the four individuals who did not wear sleep sensors on a regular basis preferred the PhyMask. Participants who were already used to wearing a wrist-worn device during sleep did not find a significant reason to change their habit. Our observations indicate the need for a follow on a large-scale survey on what forms of wearable solutions are more desirable, given that each form factor has its own tradeoffs between their comfort level and the ability to capture various physiological signals.

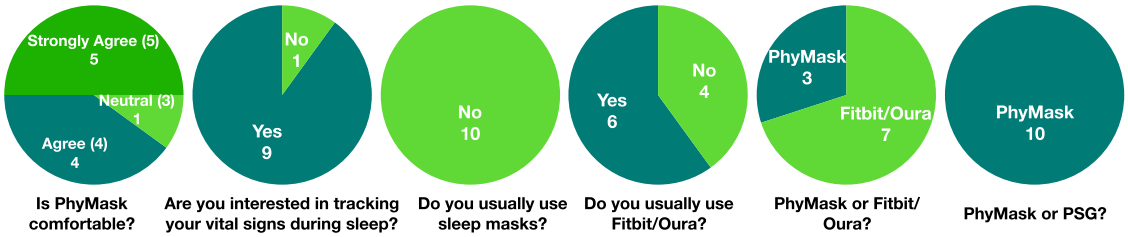

Fig. 32. Summary of subjective assessment report.

7 DISCUSSIONS AND FUTURE WORK

There are several avenues of future work that we plan to explore.

Improving robustness across users: Our current evaluation is restricted in the number of users due to the inability to recruit participants during the pandemic. We will be continuing to perform more large-scale user studies with the PhyMask to both evaluate and improve the robustness of our sensor. One key issue that we will explore is the placement of electrodes and adaptive gain control in the signal acquisition circuit such that it can work despite shifts in the device and changing signal strength. Aside from the hardware improvement, having more data would also allow us to build more generalized and powerful algorithms and enhance the robustness of the PhyMask across different individuals and challenging scenarios.

Improving the pressure sensor: Another direction we will explore is improving the sensitivity of the pressure sensor to very small amounts of pressure that are typical on the head. From the design and chemical structure point of view, there are three main factors that can be altered to increase the sensitivity of the sensors to smaller applied pressures (1 kPa). First, changing the concentration of the siloxane molecules in the solution-phase functionalization process can lead to the change in the number of charge carriers -ions- in the system and, therefore, higher sensitivity. Second, the quality of the fabric used in the active layer such as its weave density and the mesh size can play a major role in the performance of the sensor and the final number of layers used in the structure. The third factor that can improve the sensitivity of the sensor is the thickness and the weave density of the conductive fabric used as the top and bottom electrodes. These fabrics play a significant role in damping the pulses and it is anticipated that thinner fabrics can provide the capability of sensing weaker pulse pressures.

Sleep disorder monitoring: Our eventual objective is to enable the use of PhyMask in clinical-grade sleep monitoring at home to monitor sleep disorders. Our follow-on research will explore this direction further by performing sleep trials with patients with different sleep disorders like sleep apnea and REM sleep disorder.

Enhancement of comfort factor: While PhyMask incorporates all-fabric sensing elements, the electronic board has a rigid structure. In the future, we plan to use soft electronics technology [76, 77] to further maximize the PhyMask's comfort of wear.

8 CONCLUSION

In conclusion, we introduce a new all-textile system, the PhyMask, for monitoring a number of important sleep signals including EEG, EOG, respiration, heart rate, and gross body movement. Despite a plethora of commercial and research prototype sleep tracking solutions, we lack a reliable and comfortable solution that can continually monitor the whole range of sleep markers that are useful for clinical-grade sleep monitoring without impacting sleep. PhyMask bridges this gap and shows that all of these signals can be monitored by solely using soft textile-based sensors by leveraging a combination of soft hydrogel electrodes and sensitive textile-based pressure sensors. Such a system can be useful to enable high-quality clinical-grade sleep monitoring at home. Our results are very promising and demonstrate that we can measure a number of advanced sleep markers such as spindles

and K-complexes in addition to sleep stages. We can also provide robust measures of physiological features from an unconventional place, i.e., head, with high accuracy across different sleep postures.

ACKNOWLEDGMENTS

We are very grateful to Kyle Kainec and Nicholas Hathaway for taking the time to discuss the design of the PhyMask, as well as scoring the sleep data and helping us in using the sleep monitoring laboratory.

REFERENCES

[1] 2020. American Academy of Sleep Medicine. Retrieved from https://aasm.org/clinical-resources/practice-standards/.
[2] 2020. Cyton + Daisy Biosensing Boards (16-Channels). Retrieved 15 June, 2022 from https://shop.openbci.com/products/cyton-daisy-biosensing-boards-16-channel.
[3] 2020. Embla RemLogic PSG Software for sleep and micro-events annotations. Retrieved from https://neuro.natus.com/products-services/embla-remlogic-software.
[4] 2020. Go Direct Respiration Belt, Vernier. Retrieved from https://www.vernier.com/product/go-direct-respiration-belt/.
[5] 2020. Gold Cup Electrodes. Retrieved from https://shop.openbci.com/products/openbci-gold-cup-electrodes?variant=9056028163.
[6] 2020. Murata bcg mems sensor. Retrieved from https://www.mouser.com/new/Murata/murata-bcg-mems-sensor/.
[7] 2020. Single Lead Heart Rate Monitor AD8232. Retrieved from https://www.analog.com/en/products/ad8232.html.
[8] 2020. Ten20 EEG Conductive Paste. Retrieved from https://bio-medical.com/ten20-eeg-conductive-paste8oz-jars-3-pack.html.
[9] 2021. Actiwatch Spectrum Activity monitor | Philips Healthcare. Retrieved from https://www.usa.philips.com/healthcare/product/HC1046964/actiwatch-spectrum-activity-monitor.
[10] 2021. Beddit Sleep Monitor. Retrieved from https://www.beddit.com/.
[11] 2021. Dreem 2 - Sleep, finally. Retrieved from https://dreem.com/.
[12] 2021. Embletta MPR Sleep System | Natus. Retrieved from https://neuro.natus.com/products-services/embletta-mpr-sleep-system.
[13] 2021. Fitbit official site for activity trackers. Retrieved from https://www.fitbit.com/us/home.
[14] 2021. Garmin Venu®2S | Fitness Activity Tracker. Retrieved from https://www.garmin.com/en-US/p/707572.
[15] 2021. Muse™- Meditation Made Easy with the Muse Headband. Retrieved from https://choosemuse.com/.
[16] 2021. nRF52811 - Bluetooth 5.2 SoC - nordicsemi.com. Retrieved from https://www.nordicsemi.com/Products/Low-power-short-range-wireless/nRF52811.
[17] 2021. Oura Ring: Accurate Health Information Accessible to Everyone. https://ouraring.com/.
[18] 2021. Philips SmartSleep Deep Sleep Headband. Retrieved from https://www.usa.philips.com/c-e/smartsleep/deep-sleep-headband.html.
[19] 2021. Polar Sleep Plus^{TM}. Retrieved from https://www.polar.com/us-en/smart-coaching/polar-sleep-plus.
[20] 2021. SleepScore Max | The World's Most Advanced Sleep Improvement System. Retrieved from https://www.sleepscore.com/sleepscore-max-sleep-tracker/.
[21] 2021. Watch - Apple. Retrieved from https://www.apple.com/watch/.
[22] 2021. Wearable Smart EEG headband | BrainBit. Retrieved from https://brainbit.com/.
[23] 2021. WHOOP - The World's Most Powerful Fitness Membership. Retrieved from https://www.whoop.com/.
[24] Jayant N. Acharya, Abeer J. Hani, Janna Cheek, Parthasarathy Thirumala, and Tammy N. Tsuchida. 2016. American clinical neurophysiology society guideline 2: Guidelines for standard electrode position nomenclature. *The Neurodiagnostic Journal* 56, 4 (2016), 245–252.
[25] Fadel Adib, Hongzi Mao, Zachary Kabelac, Dina Katabi, and Robert C. Miller. 2015. Smart homes that monitor breathing and heart rate. In *Proceedings of the 33rd Annual ACM Conference on Human Factors in Computing Systems*. Association for Computing Machinery, New York, NY, 837–846. DOI: https://doi.org/10.1145/2702123.2702200
[26] Nicolas Alexander Alba, Robert J. Sclabassi, Mingui Sun, and Xinyan Tracy Cui. 2010. Novel hydrogel-based preparation-free EEG electrode. *IEEE Transactions on Neural Systems and Rehabilitation Engineering* 18, 4 (2010), 415–423.
[27] Yousef D. Alqurashi, Takashi Nakamura, Valentin Goverdovsky, James Moss, Michael I. Polkey, Danilo P. Mandic, and Mary J. Morrell. 2018. A novel in-ear sensor to determine sleep latency during the multiple sleep latency test in healthy adults with and without sleep restriction. *Nature and Science of Sleep* 10 (2018), 385.
[28] Committee on Sleep Medicine and Research, Board on Health Sciences Policy, Harvey R. Colten, and Bruce M. Altevogt. 2006. *Sleep Disorders and Sleep Deprivation: An Unmet Public Health Problem*. National Academies Press.
[29] Giuseppe Andreoni, Carlo Emilio Standoli, and Paolo Perego. 2016. Defining requirements and related methods for designing sensorized garments. *Sensors* 16, 6 (2016), 769.
[30] G. Balakrishnan, F. Durand, and J. Guttag. 2013. Detecting pulse from head motions in video. In *Proceedings of the 2013 IEEE Conference on Computer Vision and Pattern Recognition*. 3430–3437. DOI: https://doi.org/10.1109/CVPR.2013.440

[31] Marek Bartula, Timo Tigges, and Jens Muehlsteff. 2013. Camera-based system for contactless monitoring of respiration. In *Proceedings of the 2013 35th Annual International Conference of the IEEE Engineering in Medicine and Biology Society*. IEEE, 2672–2675.
[32] Richard B. Berry, Rita Brooks, Charlene E. Gamaldo, Susan M. Harding, C. Marcus, and Bradley V. Vaughn. 2012. The AASM manual for the scoring of sleep and associated events. *Rules, Terminology and Technical Specifications, Darien, Illinois, American Academy of Sleep Medicine* 176 (2012), 2012.
[33] Mary A. Carskadon and William C. Dement. 2005. Normal human sleep: An overview. *Principles and Practice of Sleep Medicine* 4, 1 (2005), 13–23.
[34] Sydney S. Cash, Eric Halgren, Nima Dehghani, Andrea O. Rossetti, Thomas Thesen, ChunMao Wang, Orrin Devinsky, Ruben Kuzniecky, Werner Doyle, Joseph R. Madsen, Lucia Wittner, and István Ulbert. 2009. The human K-complex represents an isolated cortical down-state. *Science* 324, 5930 (2009), 1084–1087.
[35] Nitesh V. Chawla, Kevin W. Bowyer, Lawrence O. Hall, and W. Philip Kegelmeyer. 2002. SMOTE: Synthetic minority over-sampling technique. *Journal of Artificial Intelligence Research* 16 (2002), 321–357.
[36] Nicholas I. Y. N. Chee, Shohreh Ghorbani, Hosein Aghayan Golkashani, Ruth L. F. Leong, Ju Lynn Ong, and Michael W. L. Chee. 2021. Multi-night validation of a sleep tracking ring in adolescents compared with a research actigraph and polysomnography. *Nature and Science of Sleep* 13 (2021), 177.
[37] Evan D. Chinoy, Joseph A. Cuellar, Kirbie E. Huwa, Jason T. Jameson, Catherine H. Watson, Sara C. Bessman, Dale A. Hirsch, Adam D. Cooper, Sean P. A. Drummond, and Rachel R. Markwald. 2021. Performance of seven consumer sleep-tracking devices compared with polysomnography. *Sleep* 44, 5 (2021), zsaa291.
[38] Jacob Cohen. 1960. A coefficient of agreement for nominal scales. *Educational and Psychological Measurement* 20, 1 (1960), 37–46.
[39] Joao Costa, Manuel Ortigueira, Arnaldo Batista, and T. Paiva. 2012. An automatic sleep spindle detector based on WT, STFT and WMSD. *International Journal of Biomedical and Biological Engineering* 6, 8 (2012), 397–400.
[40] Luigi De Gennaro and Michele Ferrara. 2003. Sleep spindles: an overview. *Sleep Medicine Reviews* 7, 5 (2003), 423–440.
[41] Massimiliano De Zambotti, Nicola Cellini, Aimee Goldstone, Ian M. Colrain, and Fiona C. Baker. 2019. Wearable sleep technology in clinical and research settings. *Medicine and Science in Sports and Exercise* 51, 7 (2019), 1538.
[42] Massimiliano de Zambotti, Aimee Goldstone, Stephanie Claudatos, Ian M. Colrain, and Fiona C. Baker. 2018. A validation study of fitbit charge 2™ compared with polysomnography in adults. *Chronobiology International* 35, 4 (2018), 465–476. DOI: https://doi.org/10.1080/07420528.2017.1413578
[43] Massimiliano de Zambotti, Leonardo Rosas, Ian M. Colrain, and Fiona C. Baker. 2019. The sleep of the ring: Comparison of the ŌURA sleep tracker against polysomnography. *Behavioral Sleep Medicine* 17, 2 (2019), 124–136. DOI: https://doi.org/10.1080/15402002.2017.1300587
[44] Fei Deng, Jianwu Dong, Xiangyu Wang, Ying Fang, Yu Liu, Zhaofei Yu, Jing Liu, and Feng Chen. 2018. Design and implementation of a noncontact sleep monitoring system using infrared cameras and motion sensor. *IEEE Transactions on Instrumentation and Measurement* 67, 7 (2018), 1555–1563.
[45] J. El Helou, V. Navarro, C. Depienne, E. Fedirko, E. LeGuern, M. Baulac, I. An-Gourfinkel, and C. Adam. 2008. K-complex-induced seizures in autosomal dominant nocturnal frontal lobe epilepsy. *Clinical Neurophysiology* 119, 10 (2008), 2201–2204.
[46] Tanis J. Ferman, B. F. Boeve, G. E. Smith, M. H. Silber, E. Kokmen, R. C. Petersen, and R. J. Ivnik. 1999. REM sleep behavior disorder and dementia: Cognitive differences when compared with AD. *Neurology* 52, 5 (1999), 951–951.
[47] Amir Hossein Ghaderi, Shadi Moradkhani, Arvin Haghighatfard, Fatemeh Akrami, Zahra Khayyer, and Fuat Balcı. 2018. Time estimation and beta segregation: An EEG study and graph theoretical approach. *PLoS One* 13, 4 (2018), e0195380.
[48] Ata Jedari Golparvar and Murat Kaya Yapici. 2018. Electrooculography by wearable graphene textiles. *IEEE Sensors Journal* 18, 21 (2018), 8971–8978.
[49] Ahnaf Rashik Hassan and Abdulhamit Subasi. 2017. A decision support system for automated identification of sleep stages from single-channel EEG signals. *Knowledge-Based Systems* 128 (2017), 115–124.
[50] Mohamed Abul Hassan, Aamir Saeed Malik, David Fofi, Naufal Saad, Babak Karasfi, Yasir Salih Ali, and Fabrice Meriaudeau. 2017. Heart rate estimation using facial video: A review. *Biomedical Signal Processing and Control* 38 (2017), 346–360.
[51] Nora Hennies, Matthew A. Lambon Ralph, Marleen Kempkes, James N. Cousins, and Penelope A. Lewis. 2016. Sleep spindle density predicts the effect of prior knowledge on memory consolidation. *Journal of Neuroscience* 36, 13 (2016), 3799–3810.
[52] S. Zohreh Homayounfar, Ali Kiaghadi, Deepak Ganesan, and Trisha L. Andrew. 2021. PressION: An all-fabric piezoionic pressure sensor for extracting physiological metrics in both static and dynamic contexts. *Journal of the Electrochemical Society* 168, 1 (2021), 017515. DOI: https://doi.org/10.1149/1945-7111/abdc65
[53] S. Zohreh Homayounfar, Soha Rostaminia, Ali Kiaghadi, Xingda Chen, Emerson T. Alexander, Deepak Ganesan, and Trisha L. Andrew. 2020. Multimodal smart eyewear for longitudinal eye movement tracking. *Matter* 3, 4 (2020), 1275–1293. DOI: https://doi.org/10.1016/j.matt.2020.07.030
[54] Chen-Yu Hsu, Aayush Ahuja, Shichao Yue, Rumen Hristov, Zachary Kabelac, and Dina Katabi. 2017. Zero-effort in-home sleep and insomnia monitoring using radio signals. *Proceedings of the ACM on Interactive, Mobile, Wearable and Ubiquitous Technologies* 1, 3 (2017), 1–18.

[55] Norden E. Huang, Zheng Shen, Steven R. Long, Manli C. Wu, Hsing H. Shih, Quanan Zheng, Nai-Chyuan Yen, Chi Chao Tung, and Henry H. Liu. 1998. The empirical mode decomposition and the hilbert spectrum for nonlinear and non-stationary time series analysis. *Proceedings of the Royal Society of London. Series A: Mathematical, Physical and Engineering Sciences* 454, 1971 (1998), 903–995.

[56] Syed Anas Imtiaz. 2021. A systematic review of sensing technologies for wearable sleep staging. *Sensors* 21, 5 (2021), 1562.

[57] Sogol Javaheri, Amy Storfer-Isser, Carol L. Rosen, and Susan Redline. 2008. Sleep quality and elevated blood pressure in adolescents. *Circulation* 118, 10 (2008), 1034–1040.

[58] Aude Jegou, Manuel Schabus, Olivia Gosseries, Brigitte Dahmen, Geneviève Albouy, Martin Desseilles, Virginie Sterpenich, Christophe Phillips, Pierre Maquet, Christophe Grova, and Thien Thanh Dang-Vu. 2019. Cortical reactivations during sleep spindles following declarative learning. *Neuroimage* 195 (2019), 104–112.

[59] Zhenhua Jia, Amelie Bonde, Sugang Li, Chenren Xu, Jingxian Wang, Yanyong Zhang, Richard E. Howard, and Pei Zhang. 2017. Monitoring a person's heart rate and respiratory rate on a shared bed using geophones. In *Proceedings of the 15th ACM Conference on Embedded Network Sensor Systems*. Association for Computing Machinery, New York, NY, 14 pages. DOI: https://doi.org/10.1145/3131672.3131679

[60] Korey Kam, Ankit Parekh, Ram A. Sharma, Andreia Andrade, Monica Lewin, Bresne Castillo, Omonigho M. Bubu, Nicholas J. Chua, Margo D. Miller, Anna E. Mullins, Lidia Glodzik, Lisa Mosconi, Nadia Gosselin, Kulkarni Prathamesh, Zhe Chen, Kaj Blennow, Henrik Zetterberg, Nisha Bagchi, Bianca Cavedoni, David M. Rapoport, Indu Ayappa, Mony J. de Leon, Eva Petkova, Andrew W. Varga, and Ricardo S. Osorio. 2019. Sleep oscillation-specific associations with Alzheimer's disease CSF biomarkers: Novel roles for sleep spindles and tau. *Molecular Neurodegeneration* 14, 1 (2019), 10.

[61] Seung-Gul Kang, Jae Myeong Kang, Kwang-Pil Ko, Seon-Cheol Park, Sara Mariani, and Jia Weng. 2017. Validity of a commercial wearable sleep tracker in adult insomnia disorder patients and good sleepers. *Journal of Psychosomatic Research* 97 (2017), 38–44.

[62] E. Kasasbeh, David S. Chi, and G. Krishnaswamy. 2006. Inflammatory aspects of sleep apnea and their cardiovascular consequences. *Southern Medical Journal* 99, 1 (2006), 58–68.

[63] Jessica M. Kelly, Robert E. Strecker, and Matt T. Bianchi. 2012. Recent developments in home sleep-monitoring devices. *International Scholarly Research Notices* 2012, Article 768794 (2012), 10 pages. DOI: 10.5402/2012/768794

[64] Ali Kiaghadi, Seyedeh Zohreh Homayounfar, Jeremy Gummeson, Trisha Andrew, and Deepak Ganesan. 2019. Phyjama: Physiological sensing via fiber-enhanced pyjamas. *Proceedings of the ACM on Interactive, Mobile, Wearable and Ubiquitous Technologies*. 3, 3 (2019), 29 pages. DOI: https://doi.org/10.1145/3351247

[65] Sung-Woo Kim, Kwangmuk Lee, Junyeong Yeom, Tae-Hoon Lee, Don-Han Kim, and Jae Joon Kim. 2020. Wearable multi-biosignal analysis integrated interface with direct sleep-stage classification. *IEEE Access* 8 (2020), 46131–46140.

[66] Kristen L. Knutson, Armand M. Ryden, Bryce A. Mander, and Eve Van Cauter. 2006. Role of sleep duration and quality in the risk and severity of type 2 diabetes mellitus. *Archives of Internal Medicine* 166, 16 (2006), 1768–1774.

[67] Shinjae Kwon, Hojoong Kim, and Woon-Hong Yeo. 2021. Recent advances in wearable sensors and portable electronics for sleep monitoring. *Iscience* 24, 5 (2021), 102461.

[68] Michael H. Li, Azadeh Yadollahi, and Babak Taati. 2016. Noncontact vision-based cardiopulmonary monitoring in different sleeping positions. *IEEE Journal of Biomedical and Health Informatics* 21, 5 (2016), 1367–1375.

[69] Sheng-Fu Liang, Chin-En Kuo, Yi-Chieh Lee, Wen-Chieh Lin, Yen-Chen Liu, Peng-Yu Chen, Fu-Yin Cherng, and Fu-Zen Shaw. 2015. Development of an EOG-based automatic sleep-monitoring eye mask. *IEEE Transactions on Instrumentation and Measurement* 64, 11 (2015), 2977–2985. DOI: https://doi.org/10.1109/TIM.2015.2433652

[70] Zilu Liang and Mario Alberto Chapa Martell. 2018. Validity of consumer activity wristbands and wearable EEG for measuring overall sleep parameters and sleep structure in free-living conditions. *Journal of Healthcare Informatics Research* 2, 1–2 (2018), 152–178.

[71] Zilu Liang and Takuichi Nishimura. 2017. Are wearable EEG devices more accurate than fitness wristbands for home sleep tracking? Comparison of consumer sleep trackers with clinical devices. In *Proceedings of the 2017 IEEE 6th Global Conference on Consumer Electronics*. IEEE, 1–5.

[72] Chin-Teng Lin, Chun-Hsiang Chuang, Zehong Cao, Avinash Kumar Singh, Chih-Sheng Hung, Yi-Hsin Yu, Mauro Nascimben, Yu-Ting Liu, Jung-Tai King, Tung-Ping Su, and Shuu-Jiun Wang. 2017. Forehead EEG in support of future feasible personal healthcare solutions: Sleep management, headache prevention, and depression treatment. *IEEE Access* 5 (2017), 10612–10621. DOI: https://doi.org/10.1109/ACCESS.2017.2675884

[73] Chin-Teng Lin, Lun-De Liao, Yu-Hang Liu, I-Jan Wang, Bor-Shyh Lin, and Jyh-Yeong Chang. 2011. Novel dry polymer foam electrodes for long-term EEG measurement. *IEEE Transactions on Biomedical Engineering* 58, 5 (2011), 1200–1207.

[74] Jian Liu, Yan Wang, Yingying Chen, Jie Yang, Xu Chen, and Jerry Cheng. 2015. Tracking vital signs during sleep leveraging off-the-shelf WiFi. In *Proceedings of the 16th ACM International Symposium on Mobile Ad Hoc Networking and Computing*. Association for Computing Machinery, New York, NY, 267–276. DOI: https://doi.org/10.1145/2746285.2746303

[75] Xuefeng Liu, Jiannong Cao, Shaojie Tang, and Jiaqi Wen. 2014. Wi-sleep: Contactless sleep monitoring via wifi signals. In *Proceedings of the 2014 IEEE Real-Time Systems Symposium*. IEEE, 346–355.

[76] Musa Mahmood, Shinjae Kwon, Hojoong Kim, Yun-Soung Kim, Panote Siriaraya, Jeongmoon Choi, Boris Otkhmezuri, Kyowon Kang, Ki Jun Yu, Young C. Jang, Chee Siang Ang, and Woon-Hong Yeo. 2021. Wireless soft scalp electronics and virtual reality system for motor imagery-based brain-machine interfaces. *Advanced Science* 18, 19 (2021), 2101129.

[77] Musa Mahmood, Deogratias Mzurikwao, Yun-Soung Kim, Yongkuk Lee, Saswat Mishra, Robert Herbert, Audrey Duarte, Chee Siang Ang, and Woon-Hong Yeo. 2019. Fully portable and wireless universal brain–machine interfaces enabled by flexible scalp electronics and deep learning algorithm. *Nature Machine Intelligence* 1, 9 (2019), 412–422.

[78] Urszula Malinowska, Piotr J. Durka, Katarzyna J. Blinowska, Waldemar Szelenberger, and Andrzej Wakarow. 2006. Micro-and macrostructure of sleep EEG. *IEEE Engineering in Medicine and Biology Magazine* 25, 4 (2006), 26–31.

[79] Swati Mandekar, Lina Jentsch, Dr Kai Lutz, Dr Mehdi Behbahani, and Mark Melnykowycz. 2021. Earable design analysis for sleep EEG measurements. In *Proceedings of the 2021 ACM International Joint Conference on Pervasive and Ubiquitous Computing and Proceedings of the 2021 ACM International Symposium on Wearable Computers*. 171–175.

[80] Janna Mantua, Nickolas Gravel, and Rebecca Spencer. 2016. Reliability of sleep measures from four personal health monitoring devices compared to research-based actigraphy and polysomnography. *Sensors* 16, 5 (2016), 646.

[81] Manuel Martinez and Rainer Stiefelhagen. 2012. Breath rate monitoring during sleep using near-IR imagery and PCA. In *Proceedings of the 21st International Conference on Pattern Recognition*. IEEE, 3472–3475.

[82] Georges Matar, Jean-Marc Lina, Julie Carrier, and Georges Kaddoum. 2018. Unobtrusive sleep monitoring using cardiac, breathing and movements activities: An exhaustive review. *IEEE Access* 6 (2018), 45129–45152.

[83] Dean J. Miller, Michele Lastella, Aaron T. Scanlan, Clint Bellenger, Shona L. Halson, Gregory D. Roach, and Charli Sargent. 2020. A validation study of the WHOOP strap against polysomnography to assess sleep. *Journal of Sports Sciences* 38, 22 (2020), 2631–2636. DOI: https://doi.org/10.1080/02640414.2020.1797448

[84] Fernando Moreno-Pino, Alejandro Porras-Segovia, Pilar López-Esteban, Antonio Artés, and Enrique Baca-García. 2019. Validation of fitbit charge 2 and fitbit alta HR against polysomnography for assessing sleep in adults with obstructive sleep apnea. *Journal of Clinical Sleep Medicine* 15, 11 (2019), 1645–1653.

[85] Z. Mousavi, T. Yousefi Rezaii, S. Sheykhivand, A. Farzamnia, and S. N. Razavi. 2019. Deep convolutional neural network for classification of sleep stages from single-channel EEG signals. *Journal of Neuroscience Methods* 324 (2019), 108312.

[86] Takashi Nakamura, Yousef D. Alqurashi, Mary J. Morrell, and Danilo P. Mandic. 2020. Hearables: Automatic overnight sleep monitoring with standardized in-ear EEG sensor. *IEEE Transactions on Biomedical Engineering* 67, 1 (2020), 203–212. DOI: https://doi.org/10.1109/TBME.2019.2911423

[87] Anh Nguyen, Raghda Alqurashi, Zohreh Raghebi, Farnoush Banaei-Kashani, Ann C. Halbower, and Tam Vu. 2016. A lightweight and inexpensive in-ear sensing system for automatic whole-night sleep stage monitoring. In *Proceedings of the 14th ACM Conference on Embedded Network Sensor Systems*. 230–244.

[88] Kai Niu, Fusang Zhang, Jie Xiong, Xiang Li, Enze Yi, and Daqing Zhang. 2018. Boosting fine-grained activity sensing by embracing wireless multipath effects. In *Proceedings of the 14th International Conference on Emerging Networking EXperiments and Technologies*. Association for Computing Machinery, New York, NY, 139–151. DOI: https://doi.org/10.1145/3281411.3281425

[89] Teruaki Nochino, Yuko Ohno, Takafumi Kato, Masako Taniike, and Shima Okada. 2019. Sleep stage estimation method using a camera for home use. *Biomedical Engineering Letters* 9, 2 (2019), 257–265.

[90] Danilo Pani, Alessia Dessì, Jose F. Saenz-Cogollo, Gianluca Barabino, Beatrice Fraboni, and Annalisa Bonfiglio. 2015. Fully textile, PEDOT: PSS based electrodes for wearable ECG monitoring systems. *IEEE Transactions on Biomedical Engineering* 63, 3 (2015), 540–549.

[91] Rita Paradiso, Giannicola Loriga, and Nicola Taccini. 2005. A wearable health care system based on knitted integrated sensors. *IEEE Transactions on Information Technology in Biomedicine* 9, 3 (2005), 337–344.

[92] Chanakya Reddy Patti, Ramiro Chaparro-Vargas, and Dean Cvetkovic. 2014. Automated sleep spindle detection using novel EEG features and mixture models. In *Proceedings of the 2014 36th Annual International Conference of the IEEE Engineering in Medicine and Biology Society*. IEEE, 2221–2224.

[93] Anu-Katriina Pesonen and Liisa Kuula. 2018. The validity of a new consumer-targeted wrist device in sleep measurement: An overnight comparison against polysomnography in children and adolescents. *Journal of Clinical Sleep Medicine* 14, 4 (2018), 585–591.

[94] Tauhidur Rahman, Alexander T. Adams, Ruth Vinisha Ravichandran, Mi Zhang, Shwetak N. Patel, Julie A. Kientz, and Tanzeem Choudhury. 2015. DoppleSleep: A contactless unobtrusive sleep sensing system using short-range doppler radar. In *Proceedings of the 2015 ACM International Joint Conference on Pervasive and Ubiquitous Computing*. Association for Computing Machinery, New York, NY, 39–50. DOI: https://doi.org/10.1145/2750858.2804280

[95] Rakesh Ranjan, Rajeev Arya, Steven Lawrence Fernandes, Erukonda Sravya, and Vinay Jain. 2018. A fuzzy neural network approach for automatic K-complex detection in sleep EEG signal. *Pattern Recognition Letters* 115 (2018), 74–83.

[96] M. J. L. Ravesloot, J. P. Van Maanen, L. Dun, and N. De Vries. 2013. The undervalued potential of positional therapy in position-dependent snoring and obstructive sleep apnea-a review of the literature. *Sleep and Breathing* 17, 1 (2013), 39–49.

[97] A. Roebuck, V. Monasterio, E. Gederi, M. Osipov, J. Behar, A. Malhotra, T. Penzel, and G. D. Clifford. 2013. A review of signals used in sleep analysis. *Physiological Measurement* 35, 1 (2013), R1.

[98] Soha Rostaminia, Alexander Lamson, Subhransu Maji, Tauhidur Rahman, and Deepak Ganesan. 2019. W!NCE: Unobtrusive sensing of upper facial action units with EOG-based eyewear. In *Proceedings of the ACM on Interactive, Mobile, Wearable and Ubiquitous Technologies*. 3, 1 (2019), 26 pages. DOI: https://doi.org/10.1145/3314410

[99] Iftikhar Ali Sahito, Kyung Chul Sun, Alvira Ayoub Arbab, Muhammad Bilal Qadir, and Sung Hoon Jeong. 2015. Graphene coated cotton fabric as textile structured counter electrode for DSSC. *Electrochimica Acta* 173 (2015), 164–171.

[100] Sandeep Kumar Satapathy, Satchidananda Dehuri, Alok Kumar Jagadev, and Shruti Mishra. 2019. Chapter 1 - Introduction. In *Proceedings of the EEG Brain Signal Classification for Epileptic Seizure Disorder Detection*. Sandeep Kumar Satapathy, Satchidananda Dehuri, Alok Kumar Jagadev, and Shruti Mishra (Eds.), Academic Press, 1–25. DOI: https://doi.org/10.1016/B978-0-12-817426-5.00001-6

[101] Margeaux M. Schade, Christopher E. Bauer, Billie R. Murray, Luke Gahan, Emer P. Doheny, Hannah Kilroy, Alberto Zaffaroni, and Hawley E. Montgomery-Downs. 2019. Sleep validity of a non-contact bedside movement and respiration-sensing device. *Journal of Clinical Sleep Medicine* 15, 7 (2019), 1051–1061.

[102] Suzana V. Schönwald, L. Emerson, Roberto Rossatto, Márcia L. F. Chaves, and Günther J. L. Gerhardt. 2006. Benchmarking matching pursuit to find sleep spindles. *Journal of Neuroscience Methods* 156, 1–2 (2006), 314–321.

[103] Daniel J. Schwartz, William C. Kohler, and Gillian Karatinos. 2005. Symptoms of depression in individuals with obstructive sleep apnea may be amenable to treatment with continuous positive airway pressure. *Chest* 128, 3 (2005), 1304–1309.

[104] Johanna F. A. Schwarz, Torbjörn Åkerstedt, Eva Lindberg, Georg Gruber, Håkan Fischer, and Jenny Theorell-Haglöw. 2017. Age affects sleep microstructure more than sleep macrostructure. *Journal of Sleep Research* 26, 3 (2017), 277–287.

[105] Mark J. Shensa. 1992. The discrete wavelet transform: Wedding the a trous and mallat algorithms. *IEEE Transactions on Signal Processing* 40, 10 (1992), 2464–2482.

[106] Lin Shu, Tianyuan Xu, and Xiangmin Xu. 2019. Multilayer sweat-absorbable textile electrode for EEG measurement in forehead site. *IEEE Sensors Journal* 19, 15 (2019), 5995–6005.

[107] Shiran Shustak, Lilah Inzelberg, Stanislav Steinberg, David Rand, Moshe David Pur, Inbar Hillel, Shlomit Katzav, Firas Fahoum, Maarten De Vos, Anat Mirelman, et al. 2019. Home monitoring of sleep with a temporary-tattoo EEG, EOG and EMG electrode array: A feasibility study. *Journal of Neural Engineering* 16, 2 (2019), 026024.

[108] Luc Staner, Françoise Cornette, Damien Maurice, Geoffrey Viardot, Olivier Le Bon, José Haba, Corinne Staner, Rémy Luthringer, Alain Muzet, and Jean-Paul Macher. 2003. Sleep microstructure around sleep onset differentiates major depressive insomnia from primary insomnia. *Journal of Sleep Research* 12, 4 (2003), 319–330.

[109] Shahrad Taheri. 2006. The link between short sleep duration and obesity: we should recommend more sleep to prevent obesity. *Archives of Disease in Childhood* 91, 11 (2006), 881–884.

[110] Mario Giovanni Terzano and Liborio Parrino. 2000. Origin and significance of the cyclic alternating pattern (CAP). *Sleep Medicine Reviews* 4, 1 (2000), 101–123.

[111] Robert W. Thatcher. 2012. Coherence, phase differences, phase shift, and phase lock in EEG/ERP analyses. *Developmental Neuropsychology* 37, 6 (2012), 476–496. DOI: https://doi.org/10.1080/87565641.2011.619241

[112] Jarno Tuominen, Karoliina Peltola, Tarja Saaresranta, and Katja Valli. 2019. Sleep parameter assessment accuracy of a consumer home sleep monitoring ballistocardiograph beddit sleep tracker: A validation study. *Journal of Clinical Sleep Medicine* 15, 3 (2019), 483–487.

[113] Tom Vogels, Mark Van Gastel, Wenjin Wang, and Gerard De Haan. 2018. Fully-automatic camera-based pulse-oximetry during sleep. In *Proceedings of the IEEE Conference on Computer Vision and Pattern Recognition Workshops*. 1349–1357.

[114] Ying Wang, Kenneth A. Loparo, Monica R. Kelly, and Richard F. Kaplan. 2015. Evaluation of an automated single-channel sleep staging algorithm. *Nature and Science of Sleep* 7 (2015), 101.

[115] Sompit Wanwong, Weradesh Sangkhun, S. Zohreh Homayounfar, Kwang-Won Park, and Trisha L. Andrew. 2019. Wash-stable, oxidation resistant conductive cotton electrodes for wearable electronics. *RSC Advances* 9, 16 (2019), 9198–9203.

[116] Alexandra M. V. Wennberg, Mark N. Wu, Paul B. Rosenberg, and Adam P. Spira. 2017. Sleep disturbance, cognitive decline, and dementia: A review. In *Seminars in Neurology*, Vol. 37. Thieme Medical Publishers, 395–406.

[117] Jianhong Ye, Yan Lin, Zhiwu Li, Jinshyan Lee, Al-Ahmari Abdulrahman, and Mengsi Jin. 2019. A non-invasive sleep analysis approach based on a fuzzy inference system and a finite state machine. *IEEE Access* 7 (2019), 2664–2676. DOI: https://doi.org/10.1109/ACCESS.2018.2886205

[118] Meng-Chieh Yu, Huan Wu, Jia-Ling Liou, Ming-Sui Lee, and Yi-Ping Hung. 2012. Multiparameter sleep monitoring using a depth camera. In *Proceedings of the International Joint Conference on Biomedical Engineering Systems and Technologies*. Springer, 311–325.

[119] Cüneyt Yücelbaş, Şule Yücelbaş, Seral Özşen, Gülay Tezel, Serkan Küçüktürk, and Şebnem Yosunkaya. 2018. Automatic detection of sleep spindles with the use of STFT, EMD and DWT methods. *Neural Computing and Applications* 29, 8 (2018), 17–33.

[120] Mingmin Zhao, Shichao Yue, Dina Katabi, Tommi S. Jaakkola, and Matt T. Bianchi. 2017. Learning sleep stages from radio signals: A conditional adversarial architecture. In *Proceedings of the International Conference on Machine Learning*. PMLR, 4100–4109.

Received July 2021; revised December 2021; accepted January 2022